The CCR4-NOT deadenylase complex controls Atg7-dependent cell death and heart function.

Tomokazu Yamaguchi[1,15], Takashi Suzuki[1, 15], Teruki Sato[2], Akinori Takahashi[3], Hiroyuki Watanabe[2], Ayumi Kadowaki[1], Miyuki Natsui[1], Hideaki Inagaki[4], Satoko Arakawa[5], Shinji Nakaoka[6,13], Yukio Koizumi[1], Shinsuke Seki[4], Shungo Adachi[7], Akira Fukao[8], Toshinobu Fujiwara[8], Tohru Natsume[7], Akinori Kimura[9], Masaaki Komatsu[10], Shigeomi Shimizu[5], Hiroshi Ito[2], Yutaka Suzuki[11], Josef M. Penninger[12], Tadashi Yamamoto[3], Yumiko Imai[13] and Keiji Kuba[1,14,*]

[1] Department of Biochemistry and Metabolic Science, Akita University Graduate School of Medicine, 1-1-1 Hondo, Akita 010-8543, Japan.
[2] Department of Cardiology, Akita University Graduate School of Medicine, Akita 010-8543, Japan.
[3] OIST- Okinawa Institute of Science and Technology Graduate University, Okinawa, 904-0495, Japan
[4] Bioscience Education Research Support Center, Akita University, Akita University, Akita, 010-8543, Japan.
[5] Department of Pathological Cell Biology, Medical Research Institute, Tokyo Medical and Dental University, Tokyo 113-8510, Japan.
[6] Institute of Industrial Science, The University of Tokyo, Tokyo 153-8505, Japan.
[7] Molecular Profiling Research Center for Drug Discovery, National Institute of Advanced Industrial Science and Technology, Tokyo, 135-0064, Japan.
[8] Molecular Laboratory of Biochemistry, Department of Pharmacy, Kindai University, Higashi-Osaka, 577-8502, Japan.
[9] Department of Molecular Pathogenesis, Medical Research Institute, Tokyo Medical and Dental University, Tokyo 113-8510, Japan.
[10] Department of Biochemistry, School of Medicine, Niigata University, Niigata 951-8510, Japan.
[11] Department of Medical Genome Sciences, Graduate School of Frontier Sciences, The University of Tokyo, Chiba 277-8562, Japan.
[12] IMBA -Institute of Molecular Biotechnology of the Austrian Academy of Sciences, Campus Vienna BioCenter, Vienna 1030, Austria.
[13] Laboratory of Regulation of Intractable Infectious Diseases, National Institute of Biomedical Innovation, Health and Nutrition, Ibaraki, Osaka 567-0085, Japan.

[14] JST-PRESTO, Tokyo 102-0076, Japan

[15]These authors contributed equally to this work.
*Corresponding author. Email: kuba@med.akita-u.ac.jp

Abstract

Shortening and removal of the polyadenylate (poly(A)) tail of mRNA, a process called deadenylation, is a key step in mRNA decay mediated through the CCR4-NOT (Carbon catabolite repression 4-negative on TATA-less) complex. In our investigation of the regulation of mRNA deadenylation in the heart, we found that this complex was required to prevent cell death in the heart. Conditional deletion of the CCR4-NOT complex components Cnot1 or Cnot3 resulted in the formation of autophagic vacuoles and cardiomyocyte death, leading to lethal heart failure accompanied with long QT intervals. Cnot3 bound to and shortened the poly(A) tail of the mRNA encoding the key autophagy regulator Atg7. In *Cnot3*-depleted hearts, *Atg7* expression was post-transcriptionally increased. Genetic ablation of *Atg7*, but not that of *Atg5*, increased survival and partially restored cardiac function of *Cnot1* or *Cnot3* knockout mice. We further showed that in *Cnot3*-depleted hearts, Atg7 interacted with p53 and modulated p53 activity to induce the expression of genes encoding cell death-promoting factors in cardiomyocytes, indicating that defects in deadenylation in the heart aberrantly activated Atg7 and p53 to promote cell death. Thus, mRNA deadenylation mediated by the CCR4-NOT complex is crucial to prevent Atg7-induced cell death and heart failure, suggesting a role for mRNA deadenylation in targeting autophagy genes to maintain normal cardiac homeostasis.

Introduction

Cardiovascular diseases are leading causes of death in developed countries. Coordinated transcriptional and post-transcriptional regulation of gene expression is important to maintain normal heart physiology. Dysregulation in this coordination causes and/or accompanies multiple pathologies, such as cardiomyopathy and myocardial infarction. In post-transcriptional regulation, the exonuclease-mediated degradation of the mRNA poly(A) tail, a process called deadenylation, is a key step in regulated mRNA degradation, which contributes to determining the quality and quantity of translatable mRNAs (*1, 2*). Deadenylation is mediated by the CCR4-NOT complex, which is recruited to mRNA by RNA-binding proteins (RBPs) or the miRNA repression complex, mainly by its scaffold subunit CNOT1. Following recruitment, the CCR4-NOT complex catalyzes degradation of poly(A) through the two exonuclease subunits (CNOT6 (or CNOT6L) and CNOT7 (or CNOT8)) thereby regulating gene expression (*1-4*). We have previously identified CNOT3, a scaffold subunit of the CCR4-NOT complex, as a conserved regulator of heart function in *Drosophila* and mouse (*5*). Moreover, genome wide association studies showed a strong association between SNPs in *CNOT1* or *CNOT3* and prolonged QT intervals in humans (*5-7*). The underlying mechanisms how the CCR4-NOT complex controls heart functions remained, however, elusive.

Autophagy is an evolutionally conserved mechanism in which lysosomes degrade cellular components and organelles, and this mechanism plays a crucial role in maintaining cellular energetics by recycling amino acids and fatty acids for energy

production (*8, 9*). Autophagy can be protective and is generally beneficial in the heart under basal conditions and in response to stress, such as pressure overload and ischemic injury (*10, 11*). However, the activation of autophagy in some heart pathologies induces autophagic cell death or cell death through excessive autophagy (*12, 13*). There are several molecular and functional interactions between autophagy and apoptosis or necrosis/necroptosis (*12, 14, 15*). In *Drosophila*, genetic disruption of CPEB1, a CCR4-NOT-interacting RBP, enhances autophagic cell death in oocytes through impaired deadenylation and enhanced translation of ATG12 mRNA (*16*), suggesting functional interactions between mRNA deadenylation and autophagy.

The core autophagic machinery is composed of ATG components, which contribute to autophagosome formation and the subsequent fusion of autophagosomes with lysosomes to degrade substrates. Atg7 is an ubiquitin E1-like activating enzyme which is involved in two ubiquitin like conjugation systems: covalent attachment of Atg12 to Atg5 and Atg16-like 1 (Atg16l1) and of phosphatidylethanolamine to microtubule-associated protein 1 light chain 3 (Map1lc3 or LC3) in autophagosome formation(*9*). Several autophagy gene products have also non-autophagic functions, such as the proteolytic isoform of Atg5, which induces apoptosis (*17*); the interaction of Beclin-1 with Bcl-2 (*18*), which suppresses apoptosis; and the regulation of p53 transcriptional activity by Atg7 (*19*). Here we report that in vivo inactivation of CCR4-NOT complex resulted in altered mRNA deadenylation of the key autophagy regulator *Atg7*, resulting in cardiomyocyte death and heart failure.

Results

Loss of muscle Cnot3 leads to lethal cardiomyopathy

We have previously generated whole body Cnot3 mutant mice that exhibit embryonic lethality and reported that whole body Cnot3 heterozygote mice develop heart failure (*5*). To directly examine the role of Cnot3 in cardiac muscle, we generated a *Cnot3* floxed allele through homologous recombination in ES cells (Fig. S1A). After germline transmission, *Cnot3* floxed mice were crossed with *Ckmm-Cre* Tg mice, which express Cre recombinase under the muscle creatine kinase promoter (Fig. 1A, Fig. S1B-D). Mice that lack *Cnot3* gene expression in hearts and skeletal muscles are hereafter referred to as 'Cnot3 mKO' mice. At around 3 weeks of age, Cnot3 mKO mice started to die and all of these mice were dead by 30 days after birth (Fig. 1B). Despite the loss of Cnot3 protein in skeletal muscle (Fig. S1C), the skeletal muscles of Cnot3 mKO mice appeared normal and the body weights of Cnot3 mKO mice were comparable to those of wild-type littermate mice (Fig. S1E). However, Cnot3 mKO mice had substantially enlarged and dilated hearts (Fig. 1C) that weighed more (Fig. 1D).

Echocardiography of Cnot3 mKO mice showed severe cardiac contractility defects as assessed by fractional shortening (Fig. 1E), which was accompanied by long QT intervals and various arrhythmic changes as detected by ECG analysis (Fig. 1F, Fig. S1F). Histological analysis of Cnot3 mKO mouse hearts revealed focal areas of dead cardiomyocytes with reduced cytoplasmic contents and vacuole formation (Fig. 1G). In addition, immunohistochemistry showed reduced myofibrils in Cnot3 mKO mouse

hearts (Fig. 1H), consistent with our previous observation of myofibrillar disarray in the heart tubes of *not3* RNAi *Drosophila* lines (*5*). *Cnot3* floxed mice were crossed with α*MHC-MerCreMer* Tg mice to induce cardiac muscle specific deletion of *Cnot3* at 3 month of age by tamoxifen treatment (Cnot3 cKO); adult mice with induced *Cnot3* deletion developed lethal heart failure with the same structural and functional alterations as those in the young Cnot3 mKO mice (Fig. S2A-F). Thus, muscle specific deletion of Cnot3 leads to structural and functional heart defects, ultimately resulting in lethal cardiomyopathy.

The CCR4-NOT complex is essential for cardiac homeostasis

Cnot3 is a subunit of the CCR4-NOT complex, and as expected from previous in vitro studies (*20*), it co-immunoprecipitated with Cnot1, Cnot6l and Cnot7 from cardiac extract (Fig. 2A). In the hearts of Cnot3 mKO mice at around 3 weeks old, the protein abundance of Cnot1, a major scaffold for CCR4-NOT complex organization, was markedly decreased, whereas those of the deadenylase subunits Cnot6l and Cnot7 were apparently not changed (Fig. 1A), suggesting that Cnot3 is required to maintain Cnot1 protein stability and as a consequence the integrity of the CCR4-NOT complex in cardiomyocytes.

To determine a potential role of Cnot1 in the heart, we next generated muscle-specific Cnot1 knockout mice by crossing *Cnot1* floxed mice with *Ckmm-Cre* Tg mice (these mice are hereafter referred to as ‘Cnot1 mKO’ mice) (Fig. 2B). Loss of Cnot1 in the heart muscle resulted in early lethality, with the mice dying around days 10-15 after

birth (Fig. 2C), which may be due to Cnot1 protein abundance being reduced more quickly in Cnot1 mKO mice than in Cnot3 mKO mice. Heart sizes and weights of the Cnot1 mKO mice were significantly increased (Fig. 2D), whereas the skeletal muscle weights and the body weights of Cnot1 mKO mice were unchanged (Fig. 2E). Echocardiography showed a marked decline of contractility in Cnot1 mKO mice at 10 days after birth (Fig. 2F) and ECG analysis demonstrated prolonged QT intervals in Cnot1 mKO mice (Fig. 2G). Histological analysis of the hearts of Cnot1 mKO mice revealed dying cardiomyocytes with reduced cytoplasmic contents and vacuole formation (Fig. 2H). These data show that genetic inactivation of the critical CCR4-NOT complex components Cnot1 and Cnot3 result in severe heart failure.

Autophagy protein expression is altered in Cnot3-depleted hearts, associated with cardiomyocyte death.

Cnot3 depletion in MEFs affects the expression of thousands of genes across the transcriptome (*21*). As a first step, we characterized cell death in Cnot3-depleted hearts. While the number of TUNEL-positive apoptotic cells was increased in the hearts of Cnot3 mKO mice compared with wild-type mice (Fig. S3A), Annexin V-positive apoptotic cells were not detectable among in vitro Cnot3 siRNA-transfected cardiomyocytes (Fig. S3B). However, the population of propidium iodide (PI)-positive dead cells was increased in cardiomyocytes with Cnot3 knockdown (Fig. S3B), suggesting that Cnot3 depletion triggered the death of cardiomyocytes by necrosis/necroptosis. Transmission electron microscope (TEM) analysis of Cnot3-depleted hearts showed focal areas of cardiomyocytes with disrupted actomyosin

filaments, mislocalized mitochondria, lysis of cytoplasmic contents and autophagic vacuoles (Fig. 3A), suggesting that Cnot3-deleted cardiomyocytes exhibit severe cell damage and potentially altered autophagy. The protein abundance of Ulk1, Pik3c3, Atg7 and p62 (also known as Sqstm1) was increased in Cnot3-deleted hearts, whereas LC3 (also known as Map1lc3b) protein abundance was decreased (Fig. 3B; Fig. S4A). To address whether basal autophagy activity was altered by Cnot3 depletion, we treated Cnot3 mKO mice with bafilomycin A1, a protease inhibitor for autolysosomal protein degradation. Although the protein abundance of LC3-II, the activated form of LC3, was decreased in vehicle-treated Cnot3 mKO hearts compared with WT hearts, bafilomycin A1 treatment normalized the LC3-II abundance in Cnot3 mKO hearts to values comparable to wild-type hearts (Fig. 3C; Fig. S4B). Consistently, the decrease in LC3 abundance in primary cardiomyocytes induced by Cnot3 depletion was restored by E64d and pepstatin A, a combination of protease inhibitors that prevents autolysosome activation (Fig. 3D; Fig. S4C). E64d and peptstatin A also restored LC3 abundance in mouse embryonic fibroblasts (MEFs) in which *Cnot3* was inducibly deleted by tamoxifen treatment (genotype: *Cnot3*$^{flox/flox}$*; CAG-Cre/Esr1*$^{Tg/+}$) (Fig. 3E; Fig. S4D, S4E). However, the increase in p62 abundance in Cnot3 mKO hearts was not affected by bafilomycin A1 treatment (Fig. 3C; Fig. S4B). Thus, loss of Cnot3 altered the protein abundance of several autophagy factors but had minor effects on autophagy flux.

Poly(A) tail length and the stability of mRNAs encoding autophagy factors are regulated by Cnot3.

Because the CCR4-NOT complex mediates mRNA deadenylation, we examined whether mRNAs encoding autophagy factors interacted with CCR4-NOT complex using RNA-immunoprecipitation and high-throughput sequencing (RIP-seq). RNA immunoprecipitation experiments with mouse heart lysates were performed with an antibody specific for Cnot3 and negative control IgG, and RNA from total extracts (Input) and Cnot3-immunoprecipitated samples were sequenced (Fig. 4A; Fig. S5A-C). Differentially expressed gene (DEG) analysis revealed that 983 (of 24421) protein-coding mRNAs were enriched only in Cnot3 RNA immunoprecipitations (Table S1). Gene ontology (GO) analysis showed that the mRNAs present only in Cnot3 RIP-seq DEGs were associated with the terms “transcription factor,” “histone modification,” “protein modification,” and “P-body” (Fig. 4B; Tables S2 - S4). For mRNAs encoding autophagy-encoding factors, only *Atg7* mRNA was detected in Cnot3 RNA immunoprecipitates (Fig. 4C). qPCR analysis showed that *Atg7*, *Pik3c3* and *Sqstm1* (encoding p62) mRNAs co-immunoprecipitated with Cnot3 (Fig. S5D). qPCR analysis for mRNA expression showed that the mRNA abundance of *Atg7*, *Atg5* and *Sqstm1* was not changed in Cnot3 mKO hearts (Fig. 4D). In contrast, whereas *Becn1*, *Atg12* and *Map1lc3b* (encoding LC3) mRNA abundance was decreased by Cnot3 depletion, *Ulk1* and *Pik3c3* mRNA abundance slightly increased (Fig. 4D). These results suggested that the protein abundance of Ulk1, Pik3c3, Atg7 and p62 was post-transcriptionally increased in Cnot3 mKO hearts.

We next measured the poly(A) tail length of autophagy factor-encoding mRNAs. The length of poly(A) tails for *Ulk1*, *Pik3c3*, *Atg5*, *Atg7* and *Sqstm1* mRNAs were

considerably longer in Cnot3-deleted hearts (Fig. 4E), and these longer poly(A) tails were more evident at postnatal day 18 than at postnatal day 8 (Fig. S5E), suggesting that the deadenylase activity of the CCR4-NOT complex was impaired after *Cnot3* deletion. To ask whether the longer poly(A) tail is also observed upon depletion of CCR4-NOT deadenylase subunits, we further investigated poly(A) tail length and mRNA stability in primary mouse cardiomyocytes. siRNA knockdown of Cnot3 or all the deadenylase subunits (Cnot6, Cnot6l, Cnot7 and Cnot8) efficiently decreased the mRNA and protein abundance in cardiomyocytes (Fig. S6A, S6B). The mRNA abundance of *Pik3c3*, *Atg5* and *Sqstm1* was increased in Cnot3 siRNA-treated cardiomyocytes compared to those in control siRNA-treated cells, and Cnot6/6l/7/8-depleted cardiomyocytes showed similar or greater increase in *Pik3c3*, *Atg5* and *Sqstm1* mRNA abundance (Fig. S6C). Similarly, the protein abundance of Atg5, Atg7 and p62 was increased in cardiomyocytes treated with either Cnot3 or Cnot6/6l/7/8 siRNAs (Fig. S6D). The poly(A) tails of *Ulk1*, *Pik3c3*, *Atg5*, *Atg7* and *Sqstm1* mRNAs were longer in cardiomyocytes treated with Cnot3 or Cnot6/6l/7/8 siRNAs than those in cardiomyocytes that received control siRNA (Fig. 4E; Fig. S6E). Furthermore, *Ulk1*, *Pik3c3*, *Atg5*, *Atg7* and *Sqstm1* mRNAs were more stable in cardiomyocytes treated with Cnot3 or Cnot6/6l/7/8 siRNAs than in control siRNA-treated cardiomyocytes (Fig. 4F; Fig. S6F). These results indicate that in Cnot3-depleted hearts, mRNAs encoding select autophagy factors have longer poly(A) tails and are stabilized due to decreased deadenylase activity of CCR4-NOT complex, resulting in increased protein abundance.

Loss of Atg7 improves cardiac dysfunction in CCR4-NOT complex-depleted mice.

Ulk1 and Pik3c3 are involved in autophagy initiation, and Atg7 executes autophagy by catalyzing the covalent attachment of Atg12 to Atg5 and that of phosphatidylethanolamine to LC3 with its ubiquitin E1-like enzyme activity (*9*). To ask whether the increased abundance of autophagy factors was functionally involved in heart failure of Cnot3 mKO mice, we investigated whether simultaneous knockout of Atg7 and Cnot3 genes might rescue the cardiac dysfunction of Cnot3 mKO mice. We crossed *Atg7* floxed mice and *Cnot3* floxed mice onto the *Ckmm-Cre* Tg background to delete both *Atg7* and *Cnot3* in cardiac muscle (Cnot3;Atg7 dmKO mice) (Fig. 5A). Loss of Atg7 impaired autophagosome formation as shown by a complete loss of LC3-II and an increase in p62 abundance (Fig. 5A). Although all of Cnot3 mKO mice died within 4 weeks after birth, Cnot3;Atg7 dmKO mice survived to ~7 weeks after birth (Fig. 5B). Deletion of Atg7 also significantly attenuated the increased heart weight of Cnot3 mKO mice to values comparable to control wild type mice (Fig. 5C). The impaired heart contractility and the longer QT interval in Cnot3 mKO mice were also restored to WT values in Cnot3;Atg7 dmKO mice (Fig. 5D, 5E). Histological analysis showed reduced cell death in Cnot3;Atg7 dmKO mice compared with Cnot3 mKO mice (Fig. 5F) and the reduced myofibril content in Cnot3 mKO mice was partially reversed in Cnot3;Atg7 dmKO mice (Fig. 5G). We next generated adult mice with a double knockout of Cnot3 and Atg7 (Cnot3;Atg7 dcKO mice) by crossing *Atg7* floxed mice and *Cnot3* floxed mice onto the *αMHC-MerCreMer* Tg background and treating the resulting mice with tamoxifen. Adult Cnot3;Atg7 dcKO mice survived for longer and

showed increased heart contractility and reduced cardiomyocyte death compared to the single Cnot3 cKO mice (Fig. S7A-F) at 14 days after tamoxifen treatment. To clarify the effects of Cre overexpression, we generated the Cnot3;Atg7 dcKO mice homozygous for *αMHC-MerCreMer* Tg, namely double-Cre Cnot3;Atg7 dcKO mice (genotype: $Cnot3^{f/f};Atg7^{;f/f};\alpha MHC\text{-}MerCreMer^{Tg/Tg}$) and compared them with the mice heterozygous for *αMHC-MerCreMer* Tg; single-Cre Cnot3;Atg7 dcKO mice (genotype: $Cnot3^{f/f};Atg7^{;f/f};\alpha MHC\text{-}MerCreMer^{Tg/+}$) (Fig. S7D). The phenotypic rescue of cardiac dysfunction in adult Cnot3 cKO mice by double knockout of Cnot3 and Atg7 (Cnot3;Atg7 dcKO mice) was comparable between double-Cre and single-Cre expressing mice (Fig. S7E), indicating that over-expression of Cre recombinase did not affect the observed phenotype. In addition, overexpression of *ATG7* increased the population of PI-positive dead cells in Cnot3 siRNA-transfected cardiomyocytes but not in control siRNA-transfected cells (Fig. S8A, S8B). Furthermore, we deleted both Cnot1 and Atg7 on the *Ckmm-Cre* Tg background in cardiac muscle (Cnot1;Atg7 dmKO mice (genotype: $Cnot3^{f/f};Atg7^{;f/f};Ckmm\text{-}Cre^{Tg/+}$)) (Fig. 6A). Cnot1;Atg7 dmKO mice survived longer than Cnot1 mKO mice (Fig. 6B). Deletion of Atg7 significantly attenuated the impaired heart contractility and longer QT interval in Cnot1 mKO mice to wild type values (Fig. 6C, 6D). Histological analysis showed reduced cell death in Cnot1;Atg7 dmKO mice compared with Cnot1 mKO mice (Fig. 6E).

To explore if canonical autophagy was responsible for the rescue of heart failure in Cnot3 mutant mice, we also generated *Atg5* flox*, Cnot3* flox and *Ckmm-Cre* Tg mice (Cnot3;Atg5 dmKO mice) (Fig. 5A; Fig. S9A). Similar to Atg7, loss of Atg5 also

critically impaired autophagosome formation in the heart (Fig. 5A), which is consistent with previous studies showing essential roles of Atg5 as well as Atg7 in canonical autophagy (*22*). However, double knockout of Atg5 and Cnot3 (Cnot3;Atg5 dmKO) did not rescue the reduced survival, increased heart weight, impaired contractility, and conduction defects observed in the single Cnot3 mKO mice (Fig. S9B-E), indicating that autophagy per se was not responsible for the rescue of the Cnot3 KO heart phenotype. These data indicate that Atg7 promotes cardiac dysfunction of Cnot3 mKO mice independently of the canonical autophagy pathway.

Nuclear Atg7 regulates p53 activity to induce the expression of cell death genes in Cnot3-depleted cardiomyocytes.

Consistent with previous studies on CCR4-NOT depletion in cancer cells and B cells (*20, 23*), p53 protein abundance was increased in the hearts of Cnot3 mKO mice (Fig. 7A). In response to starvation, Atg7 localizes to nucleus and promotes p53-mediated transcription of *p21*, which encodes a cell cycle inhibitor, in fibroblasts or HCT116 colon carcinoma cells (*19*). We thus examined the localization of Atg7 proteins in Cnot3 KO mouse embryonic fibroblasts (MEFs). Immunocytochemistry showed that Atg7 and p53 were detected in the nucleus of Cnot3 KO MEFs (Fig. 7B; Fig. S10A), and subcellular fractionation also showed that the nuclear amounts of both Atg7 and p53 were increased in Cnot3 KO MEFs compared with control cells (Fig. 7C). In Cnot3 siRNA-transfected cardiomyocytes the nuclear localization of Atg7 and p53 was also increased compared with control siRNA-transfected cardiomyocytes (Fig. 7D; Fig. S10B). Atg7 and p53 coimmunoprecipitated from Cnot3 mKO heart lysates, indicating

that Atg7 and p53 interacted in Cnot3-depleted hearts (Fig. 7E; Fig. S10C). Moreover, simultaneous transfection of p53 siRNA or Atg7 siRNA with Cnot3 siRNA decreased the numbers of PI-positive dead cardiomyocytes (Fig. 7F; Fig. S10D-F), suggesting that p53 is involved in cell death in Cnot3-depleted hearts.

We next examined p53 target gene expression in Cnot3-deleted hearts. Although ATG7 induces *p21* expression in nutrient-deprived cells (*19*), *p21* expression was not significantly increased in Cnot3-depleted cardiomyocytes, which was also not affected by additional deletion of Atg7 (Fig. 7G). In contrast, genes encoding cell death factors such as *Puma*, *Bax* and *Ripk3* showed increased expression in the hearts of Cnot3 mKO mice (Fig. 7G). The increased mRNA expression of *Puma* and *Ripk3* but not *Bax* was decreased to varying extents by double knockout of Cnot3 and Atg7 (Fig. 7G). Moreover, Puma protein abundance was consistently increased in Cnot3-deleted hearts but decreased by additional knockout of Atg7 (Fig. S11A). Puma protein abundance is largely regulated at the transcriptional level through both p53-dependent and p53-independent mechanisms (*24*). Chromatin immunoprecipitation (ChIP) showed that in Cnot3 KO MEFs, Atg7 was bound to the genomic region close to the transcriptional start site of the *Puma* and *Ripk3* genes (Fig. S11B), overlapping the region where p53 binds and induces gene expression (*24*) (Fig. S11B). Moreover, siRNA-mediated knockdown of p53 decreased the binding of Atg7 protein to the *Puma* and *Ripk3* gene loci in Cnot3 KO MEFs (Fig. 7H; Fig. S11C). Cnot3 RIP-seq analysis using mouse heart lysates (Fig. 4A, B; Table S1) showed that Cnot3 protein bound to *Puma* mRNA, but not *Bax*, *Ripk1* and *Ripk3* mRNAs (Fig. S11D). *Puma* mRNA

expression was not stabilized but markedly increased by Cnot3 depletion in cardiomyocytes (Fig. S11E, S11F), suggesting that the increase in *Puma* expression in Cnot3-deleted hearts was primarily mediated through increased transcription. These results indicate that under CCR4-NOT-depleted conditions, Atg7 regulates p53 activity to induce expression of cell death-associated genes.

Discussion

In this study, we demonstrated that mRNA deadenylation of the autophagy regulator Atg7 through the CCR4-NOT complex was crucial to maintain cardiomyocyte survival, cardiac contractility and proper QT intervals. Cnot3 interacted with nearly one thousand mRNAs including *Atg7* and regulated poly(A) tail shortening and mRNA decay of *Atg7* mRNA. Loss of Cnot3 led to increased expression and non-canonical activation of Atg7 to promote p53-induced expression of *Puma* and *Ripk3*, thereby accelerating cardiomyocyte death.

Although loss of Cnot3 had minor effects on canonical autophagy process, our genetic data revealed a molecular connection between Cnot3 and Atg7, in which simultaneous deletion of Atg7 and Cnot3 markedly slowed the damage to Cnot3-deleted hearts. In autophagy flux measurements, we observed discrepant changes in autophagy markers. Decreased LC3-II abundance in Cnot3 mKO hearts was restored to control values with bafilomycin A1, which was indicative of increased autophagy flux, but counter to this observation was the lack of further increase in p62 abundance. These finding may point to previously unknown pathways and biology. Indeed, in Cnot3-mutated cells, Atg7 bound to p53 in the nucleus where it localized to transcriptional start sites of *Puma* and *Ripk3*, close to the p53-binding motif. The interaction of Atg7 and p53 in CCR4-NOT-depleted cardiomyocytes was likely involved in inducing cell death, whereas the same interaction occurring in nutrient-deprived proliferating cells halts cell cycle progression and thereby prevent cell damage (*19*). In addition, inducible overexpression of *Atg7* in the adult hearts does not induce overt cell death

phenotypes (*25*). We thus anticipated that overexpression of Atg7 alone was not sufficient to induce cardiomyocyte death, and indeed Atg7-mediated cell damage required Cnot3 depletion. We assume that impaired mRNA deadenylation and/or dysregulation of other autophagy genes were necessary for Atg7-mediated cell damage. The mechanism by which CCR4-NOT depletion facilitates binding of Atg7 and p53 proteins to the genomic regions of *Puma* and *Ripk3* is currently unknown. Since our electron microscopy analysis also showed abnormal structures of nuclear membranes and RIP-seq analysis showed that GO terms for transcription factors were enriched in Cnot3-bound RNAs, CCR4-NOT depletion might alter chromatin architecture and accessibility to transcription factors. Nevertheless, our findings strengthen the biological relevance of Atg7 and p53 interactions and may warrant further studies on Atg7 functions.

Puma and Ripk3 promote necrosis and/or apoptosis of cardiomyocytes in mouse heart failure models (*26-28*). Deletion of Puma attenuates cardiomyocyte apoptosis induced by pressure overload stress (*27*). However, we did not find evidence that Cnot3 depletion increased cardiomyocyte apoptosis in vitro or in vivo. However, reduced cytoplasmic contents and vacuole formation in cardiomyocytes in vivo and increased population of PI-positive cells in vitro suggested the involvement of necrosis and autophagic cell death in Cnot3-deleted cardiomyocytes. Thus, necrosis/necroptosis may be the primary cause of death in Cnot3-depleted cardiomyocytes. The necroptotic kinases Ripk1 and Ripk3 are involved in ischemia reperfusion injury of the heart (*26, 29*), and in this study we showed that *Ripk3* expression was increased by Atg7 in

Cnot3-depleted hearts, which is mechanistically distinct from the Cnot3-mediated decrease in *Ripk1* expression through mRNA deadenylation in MEFs (*21*). These results suggest the existence of heart-specific mechanisms of cell survival. We have previously reported that in the heart failure model induced by pressure overload, Cnot3 heterozygous mice show enhanced cardiac fibrosis, which represents cardiomyocyte damage as well as tissue remodeling (*5*). Thus, we speculate that Cnot3 is crucial for survival of cardiomyocytes under pathological conditions. However, long QT interval and arrhythmic changes in Cnot3 mKO mice may or may not be secondary to the advanced myocardial dysfunction and cell death. Though detailed molecular mechanisms need to be further explored, our genetic models of Cnot1 or Cnot3 deficiency in hearts demonstrate the importance of the CCR4-NOT complex in cardiac homeostasis.

The CCR4-NOT complex regulates gene expression through both transcriptional and post-transcriptional mechanisms (*1*). Our data indicate that the expression of *Ulk1*, *Pik3c3*, *Atg7* and *Sqstm1* was post-transcriptionally suppressed by the CCR4-NOT complex through decreased mRNA stability and possibly translation suppression. Why *Atg7*, out of almost one thousand RNAs bound to Cnot3 and/or CCR4-NOT target genes, is important for cell death in Cnot3-depleted hearts is currently unknown, but the enrichment of transcription factors in Cnot3-bound mRNAs may be related to the connection between the phenotypes caused by loss of Cnot3 and Atg7-regulated p53 transcriptional activity. In the mammalian CCR4-NOT complex, CNOT1 and CNOT3 form a stable core bound to other subunits but do not directly bind to mRNAs. The

recognition of autophagy factor-encoding mRNAs by CCR4-NOT complex is hence likely mediated through RBPs which interact with the core CCR4-NOT complex. Future work will be required to identify the RBPs that bind to mRNAs that encode autophagy factors and to the CCR4-NOT complex.

In summary, our findings linking mRNA deadenylation to *Atg7* gene regulation uncover a cell survival pathway required for cardiac homeostasis. Modulating poly(A) mRNA tail length and/or targeting the pro-death effect of nuclear Atg7 might be candidate strategies for treating heart diseases. Furthermore, because compounds to activate canonical autophagy are being developed to treat various diseases, our results might be serve as a cautionary warning for the potential side effects of such compounds and could contribute to the development of better autophagy-targeting therapeutics.

Materials and Methods

Cardiac gene knockout of *Cnot3* or *Cnot1* in mice

A targeting vector was constructed to flank exons 2 and 3 of the murine *Cnot3* gene by loxP. The linearized construct was electroporated into A9 embryonic stem (ES) cells derived from 129/Ola and C57BL/6J hybrids. The correctly-targeted ES cell clones were processed to blastocyst injection to generate chimeric mice, which were then crossed with FLPe transgenic mice to delete Neo-cassette and obtain Cnot3 flox allele. Cnot3 flox mice were further crossed with muscle creatine kinase promoter-Cre Tg mice (*Ckmm-Cre* Tg mice (*31*)) to generate muscle-specific Cnot3 knockout (Cnot3 mKO) mice. Heart-specific tamoxifen-inducible Cnot3 knockout mice (Cnot3 cKO) were generated by crossing *Cnot3* flox mice with α*MHC-MerCreMer* Tg mice, and deletion of Cnot3 in adult mice were induced by 5 consecutive days of intraperitoneal injection of 4-hydroxy-tamoxifen (20 mg/kg/day, Sigma H6278), as described previously(*32*). For conditional deletion of Cnot3 in MEFs, we generated CAG promoter driven tamoxifen-inducible Cnot3 knockout mice (*Cnot3*$^{f/f}$; *CAG-cre/Esr1*5Amc*$^{Tg/+}$ mice) (*33*). Double mutant mice carrying mutations in both Cnot3 and Atg7 (Cnot3;Atg7 dmKO or *Cnot3*$^{f/f}$*; Atg7*$^{f/f}$*; Ckmm-Cre* Tg mice) (Cnot3;Atg7 dcKO or *Cnot3*$^{f/f}$*; Atg7*$^{f/f}$*;* α*MHC-MerCreMer* Tg mice) or in both Cnot3 and Atg5 (Cnot3;Atg5 dmKO or *Cnot3*$^{f/f}$*; Atg5*$^{f/f}$*; Ckmm-Cre* Tg mice) were generated and intercrossed more than 10 times (*22, 34*). *Cnot1* flox mice were generated by homologous recombination in ES cells, in which loxPs flank exons 21-22 of the *Cnot1* gene (RIKEN, Accession No. CDB0916K), and muscle-specific Cnot1 knockout (Cnot1 mKO) mice were generated similarly by crossing *Cnot1* flox mice with *Ckmm-*

Cre Tg mice. A residual reactivity to the antibody or qPCR amplification of genes in the mKO hearts is likely derived from the non-muscle cells in the heart (Fig. 2B; Fig. 6A). Mice were genotyped by PCR and Southern blotting and maintained at the animal facilities of Akita University Graduate School of Medicine. All animal experiments conformed to the Guide for the Care and Use of Laboratory Animals published by the US National Institutes of Health (NIH Publication No. 85-23, revised 1996). Approvals for the experiments were granted by the ethics review board of Akita University.

Echocardiography and ECG measurements

Echocardiographic measurements were performed as described (*35*). Briefly, mice were anesthetized with isoflurane (1%)/oxygen, and echocardiography was performed using Vevo770 equipped with a 30-MHz linear transducer. Fractional shortening (FS) was calculated as follows: [(LVEDD – LVESD)/LVEDD] x 100. We used 2D-guided M-mode measurements to determine % FS. The heart was first imaged in 2D mode in the parasternal short-axis view. From this view, an M-mode cursor was positioned perpendicular to the interventricular septum and posterior wall of the left ventricle at the level of the papillary muscles. M-mode images were obtained for measurement of wall thickness and chamber dimensions with the use of the leading-edge convention adapted by the American Society of Echocardiography. For measurements of ECG (electrocardiography), the anesthetized mice were placed on a heating pad with continuous monitoring of body temperature for three-lead ECG measurements in lead II for over 10 min using pad electrodes and a PowerLab 26T system (AD Instruments). Recordings (16 bit, 2 kHz/channel) were analyzed using the LabChart v7.0 program

(AD Instruments) and filtered between 0.5 and 500 Hz. Corrected QT (QTc) intervals were obtained using the formula $QT/(RR/100)^{1/2}$, as described (*36*).

Histology

For histology, hearts were arrested with 1 M KCl, fixed with 10% formalin, and embedded in paraffin. 5 μm-thick sections were then cut and stained with hematoxylin and eosin (H&E). To detect apoptotic cells, TUNEL assay was performed using ApopTag Peroxidase In Situ Apoptosis Detection Kit (Chemicon). To detect fibrotic areas, sections were stained with Masson-Trichrome. To visualize filamentous actin (F-actin) as myofibrils, frozen hearts were cryo-sectioned with thickness of 8-10 μm and probed with Alexa546-labeled phalloidin and DAPI (Molecular Probes). For electron microscopy analyses, heart tissues were fixed by a conventional method. Fixed samples were embedded in Epon 812, and thin sections were then cut and stained with uranyl acetate and lead citrate for observation under a Jeol-1010 electron microscope (Jeol) at 80 kV (*37*).

RNA analyses

Tissue RNA was extracted using TRIzol reagent (Invitrogen), and RNA from cells was extracted with RNeasy Mini Kit (Qiagen). For real-time qRT-PCR, cDNA was synthesized using the PrimeScript RT reagent kit (TAKARA), and real-time PCR was run in 96 well plates using a SYBR Premix ExTaq II (TAKARA) according to the instructions of the manufacturer. Relative gene expression was quantified using the Thermal Cycler Dice Real Time System II software (TAKARA). All primers used in

qRT-PCR are listed in Table S5. To assess mRNA stability, cells were treated with actinomycin D (2.5 μg/ml, Wako). Total RNA was extracted at indicated time points after actinomycin D treatment, and subjected to qRT-PCR. Measurement of poly (A) length was performed as described previously(*38*). Briefly, heart RNAs (150 ng) were subjected to reverse transcription with oligo(dT) anchor primer (5'-GCGAGCTCCGCGGCCGCGTTTTTTTTTTTT-3') using Cloned AMV First-Strand cDNA Synthesis Kit (Invitrogen). The 3' ends of synthesized cDNAs were amplified with oligo(dT) anchor and gene specific primers.

RIP-seq

RNA/CNOT3 complexes were immunoprecipitated from mouse heart lysates using anti-CNOT3 antibody (*21*) or control IgG (MBL) antibodies as described (*39*). RNAs in immunoprecipitates were purified with RIP-Assay Kit (MBL). Total RNA extracted from heart lysates (Input) or immunoprecipitated with control IgG or anti-CNOT3 IgG was used for RNA-seq library preparation with TruSeq Strand mRNA Sample Prep kit (Illumina). 36 base-pair single-end read RNA-seq was performed with Hiseq3000 (Illumina). For data analysis we employed a conventional method commonly applied to RNA-seq data to process RIP-seq data (*40*). Raw FASTQ files were assessed to remove low quality reads by Trimmomatic version 0.3.6 (*41*). High quality reads were subsequently aligned to UCSC mm10 as the reference genome by Bowtie2 version 2.2.5 with Tophat version 2.1.0. Raw read count data were extracted, normalized and analyzed to obtain DEGs by R Bioconductor version 3.5 packages Rsubread and edgeR. The tools used have been described previously (*42*). The read count data

showed sufficient sequencing depth in terms of the total number assigned reads and good correlations among technical replicates (Fig. S5B and S5C). Genes were detected as differentially expressed if a false discovery rate (FDR) calculated by the Benjamini-Hochberg method was less than 0.05, gene expression for the mean value of Input samples (two replicates) measured by counts-per-million value is greater than 0.1 and the fold-change over Input is greater than $2^{0.5}$=1.414. GO-enrichment analysis was implemented by R Bioconductor package clusterProfiler (*43*). GO terms were selected by *p*-value with cutoff threshold 0.01. The RIP-seq data generated from Cnot3 RIP (n=2 independent experiments), control IgG RIP (n=2 independent experiments), and RNA from total extracts (n=2 independent experiments) have been deposited at NCBI's Gene Expression Omnibus (GEO, http://www.ncbi.nlm.nih.gov/geo/) under the accession number GSE103629.

Cell cultures

Primary cardiomyocytes were isolated from prenatal mouse hearts of wild type mice as described previously (*44*). Briefly, hearts were excised and rapidly minced into 3 or 4 pieces and digested with collagenase (Wako) for 45 min at 35°C. Cardiomyocytes were collected, pre-plated to exclude non-cardiomyocytes, and plated on gelatinized culture dishes or plates with siRNAs for control, Cnot3, Atg7, p53 or combinations of Cnot6, Cnot6l, Cnot7 and Cnot8 siRNAs. siRNA target sequences are listed in Table S6. Twenty four hours after plating, control plasmid or pCMV-hATG7 (*45*) was transfected. At 72 hours after plating, cardiomyocytes were subjected to various assays. For inducible deletion of Cnot3 in MEFs, MEFs were isolated from 13.5 dpc

embryos from the crossing of *Cnot3*$^{f/f}$;*CAG-Cre/Esr1*5Amc*$^{Tg/+}$ mice and *Cnot3*$^{f/f}$ mice, and the genotypes were determined by PCR. When plating, the *Cnot3*$^{f/f}$;*CAG-Cre/Esr1*5Amc*$^{Tg/+}$ MEFs (passage 4-7) were treated with 2 μM 4-hydroxy-tamoxifen (4-OHT) to obtain Cnot3 KO MEFs, and vehicle-treated *Cnot3*$^{f/f}$;*CAG-Cre/Esr1*5Amc*$^{Tg/+}$ MEFs or *Cnot3*$^{f/f}$ MEFs served as wild type MEFs. At 48 or 72 hours after plating, MEFs were harvested for various assays.

Immunoprecipitation and Western blot

Heart proteins were extracted with a TNE lysis buffer (50 mM Tris, 150 mM NaCl, 1 mM EDTA, 1% NP40, protease inhibitor (complete Mini, Roche), 100 mM NaF, 2 mM Na_3VO_4), as previously described(*44*). Heart lysates were precleared with protein G-Sepharose (GE healthcare) for 1 hour at 4°C and proteins in supernatant were immunoprecipitated with anti-CNOT3 (clone 4B8; Abnova), anti-ATG7 (*45*), anti-p53 (Cell Signaling 1C12), or control IgG at 4°C overnight. Immune complexes were washed five times with TNE lysis buffer followed by mixing with LDS sample buffer (Invitrogen). After sonication and denaturation with LDS sample buffer (Invitrogen) at 70°C, proteins were electrophoresed on NuPAGE bis-tris precast gels (Invitrogen) and transferred to nitrocellulose membranes (0.2 μm pore, Invitrogen). Membranes were probed with following antibodies; CNOT1, CNOT3, CNOT6L, CNOT7 and ATG7 antibodies described previously (*45-47*) and commercially obtained CNOT3 (clone 4B8; Abnova), Ulk1 (Cell Signaling D8H5), Pik3c3 (Cell Signaling 3811), Becn1 (Cell Signaling D40C5), ATG5 (Sigma A0731), hnRNPC (Sigma R5028), LC3 (Cell Signaling 2775), Puma (Cell Signaling 14570), p62 (MBL PM045), α-Tubulin (Sigma

T5168) and GAPDH (Cell Signaling 14C10) antibodies. The bands were visualized with ECL reagent (GE healthcare) using ChemiDoc Touch Imaging System (Bio-Rad). Image Lab software was used to quantify band intensity.

Immunocytochemistry

Mouse cardiomyocytes on LabTek chambers (Thermo Scientific, 177437) or MEFs on cover slips were fixed with 4% paraformaldehyde and incubated with antibodies for ATG7 (*45*), p53 (Cell Signaling 1C12), LC3 (Cell Signaling 2775) or p62 (MBL PM045) and then incubated with appropriate secondary antibodies. LabTek chambers were mounted with mounting medium containing DAPI. Apoptotic cells were detected using Annexin V-FITC Apoptosis Detection Kit (Biovision) according to the manufacturer's instructions. Necrotic/necroptotic cells were detected by PI incorporation. Cells were treated with 5 μg/ml of PI (Sigma) and 100 μg/ml of Hoechst (Thermo Scientific) for 10 min at room temperature and analyzed using fluorescence microscopy. The cell death rate was calculated as ratio of PI to Hoechst incorporation in nuclei. Images were analyzed using multiphoton laser microscopy (A1R MP, Nikon) or fluorescence microscopy (BZ9000, Keyence).

ChIP assay

Wild type and Cnot3 KO MEFs at 72 hr after 4-OHT treatment were crosslinked with 1% paraformaldehyde for 5 minutes, quenched with glycine, cell lysates harvested, and chromatin DNAs were shared to 300-600 bp size by using the Picoruptor (Diagenode). ChIP assays were performed using the ChIP-IT (Active Motif) and IgG

(Active Motif) used as a negative control. Anti-Atg7 or anti-p53 antibodies were used to immunoprecipitate the DNA/protein complex. Crosslink reversed samples were treated with Proteinase K and the DNA purified and analyzed by qPCR. The qPCR primers were designed in the region of *Puma* genomic locus (+253 ~ +485 from the transcriptional start site) and *Ripk3* genomic locus (-698 ~ -543 from the transcriptional start site).

Measurement of autophagy flux

Cardiac autophagy flux was determined as previously described (*48*). Briefly, mice were intraperitoneally injected with Bafilomycin A1 (6 μmol/kg, LC Laboratories) 30 min before sacrifice. To determine autophagy flux in primary cardiomyocytes and MEFs, cells were treated with 10 μg/ml of E64d and 10 μg/ml of pepstatin A (Peptide Institute) for 24 hour at 37°C. LC3-II and p62 protein abundance and LC3 puncta were detected by western blotting and immunocytochemistry, respectively, as markers of autophagy flux.

Statistical analyses. Data are presented as mean values ± SEM. Normally distributed data were analyzed by an unpaired *t*-test. Data not normally distributed were analyzed using the Mann-Whitney test. $P < 0.05$ was considered significant.

Supplementary Materials

References and Notes

1. M. A. Collart, O. O. Panasenko, The Ccr4--not complex. *Gene* **492**, 42-53 (2012).
2. E. Wahle, G. S. Winkler, RNA decay machines: deadenylation by the Ccr4-not and Pan2-Pan3 complexes. *Biochim Biophys Acta* **1829**, 561-570 (2013).
3. J. E. Miller, J. C. Reese, Ccr4-Not complex: the control freak of eukaryotic cells. *Crit Rev Biochem Mol Biol* **47**, 315-333 (2012).
4. S. Jonas, E. Izaurralde, Towards a molecular understanding of microRNA-mediated gene silencing. *Nature reviews. Genetics* **16**, 421-433 (2015).
5. G. G. Neely *et al.*, A global in vivo Drosophila RNAi screen identifies NOT3 as a conserved regulator of heart function. *Cell* **141**, 142-153 (2010).
6. C. Newton-Cheh *et al.*, Common variants at ten loci influence QT interval duration in the QTGEN Study. *Nature genetics* **41**, 399-406 (2009).
7. A. Pfeufer *et al.*, Common variants at ten loci modulate the QT interval duration in the QTSCD Study. *Nature genetics* **41**, 407-414 (2009).
8. L. Galluzzi, F. Pietrocola, B. Levine, G. Kroemer, Metabolic control of autophagy. *Cell* **159**, 1263-1276 (2014).
9. N. Mizushima, M. Komatsu, Autophagy: renovation of cells and tissues. *Cell* **147**, 728-741 (2011).
10. S. Lavandero, M. Chiong, B. A. Rothermel, J. A. Hill, Autophagy in cardiovascular biology. *The Journal of clinical investigation* **125**, 55-64 (2015).
11. A. Nakai *et al.*, The role of autophagy in cardiomyocytes in the basal state and in response to hemodynamic stress. *Nat Med* **13**, 619-624 (2007).
12. G. Kroemer, B. Levine, Autophagic cell death: the story of a misnomer. *Nature reviews. Molecular cell biology* **9**, 1004-1010 (2008).
13. H. Zhu *et al.*, Cardiac autophagy is a maladaptive response to hemodynamic stress. *The Journal of clinical investigation* **117**, 1782-1793 (2007).
14. D. R. Green, L. Galluzzi, G. Kroemer, Mitochondria and the autophagy-inflammation-cell death axis in organismal aging. *Science* **333**, 1109-1112 (2011).
15. S. Shimizu *et al.*, Role of Bcl-2 family proteins in a non-apoptotic programmed cell death dependent on autophagy genes. *Nat Cell Biol* **6**, 1221-1228 (2004).
16. P. Rojas-Rios *et al.*, Translational Control of Autophagy by Orb in the Drosophila Germline. *Dev Cell* **35**, 622-631 (2015).
17. S. Yousefi *et al.*, Calpain-mediated cleavage of Atg5 switches autophagy to apoptosis. *Nat Cell Biol* **8**, 1124-1132 (2006).
18. S. Pattingre *et al.*, Bcl-2 antiapoptotic proteins inhibit Beclin 1-dependent autophagy. *Cell* **122**, 927-939 (2005).
19. I. H. Lee *et al.*, Atg7 modulates p53 activity to regulate cell cycle and survival during metabolic stress. *Science* **336**, 225-228 (2012).
20. S. Mittal, A. Aslam, R. Doidge, R. Medica, G. S. Winkler, The Ccr4a (CNOT6) and Ccr4b (CNOT6L) deadenylase subunits of the human Ccr4-Not complex contribute to the prevention of cell death and senescence. *Mol Biol Cell* **22**, 748-758 (2011).
21. T. Suzuki *et al.*, CNOT3 suppression promotes necroptosis by stabilizing mRNAs for cell death-inducing proteins. *Sci Rep* **5**, 14779 (2015).

22. T. Hara *et al.*, Suppression of basal autophagy in neural cells causes neurodegenerative disease in mice. *Nature* **441**, 885-889 (2006).
23. T. Inoue *et al.*, CNOT3 contributes to early B cell development by controlling Igh rearrangement and p53 mRNA stability. *The Journal of experimental medicine* **212**, 1465-1479 (2015).
24. J. Yu, L. Zhang, PUMA, a potent killer with or without p53. *Oncogene* **27 Suppl 1**, S71-83 (2009).
25. M. S. Bhuiyan *et al.*, Enhanced autophagy ameliorates cardiac proteinopathy. *The Journal of clinical investigation* **123**, 5284-5297 (2013).
26. M. Luedde *et al.*, RIP3, a kinase promoting necroptotic cell death, mediates adverse remodelling after myocardial infarction. *Cardiovascular research* **103**, 206-216 (2014).
27. A. Mandl, L. Huong Pham, K. Toth, G. Zambetti, P. Erhardt, Puma deletion delays cardiac dysfunction in murine heart failure models through attenuation of apoptosis. *Circulation* **124**, 31-39 (2011).
28. A. Toth *et al.*, Targeted deletion of Puma attenuates cardiomyocyte death and improves cardiac function during ischemia-reperfusion. *American journal of physiology. Heart and circulatory physiology* **291**, H52-60 (2006).
29. M. I. Oerlemans *et al.*, Inhibition of RIP1-dependent necrosis prevents adverse cardiac remodeling after myocardial ischemia-reperfusion in vivo. *Basic Res Cardiol* **107**, 270 (2012).
30. J. Tay, J. D. Richter, Germ cell differentiation and synaptonemal complex formation are disrupted in CPEB knockout mice. *Dev Cell* **1**, 201-213 (2001).
31. J. C. Bruning *et al.*, A muscle-specific insulin receptor knockout exhibits features of the metabolic syndrome of NIDDM without altering glucose tolerance. *Mol Cell* **2**, 559-569 (1998).
32. D. S. Sohal *et al.*, Temporally regulated and tissue-specific gene manipulations in the adult and embryonic heart using a tamoxifen-inducible Cre protein. *Circ Res* **89**, 20-25 (2001).
33. S. Hayashi, A. P. McMahon, Efficient recombination in diverse tissues by a tamoxifen-inducible form of Cre: a tool for temporally regulated gene activation/inactivation in the mouse. *Dev Biol* **244**, 305-318 (2002).
34. M. Komatsu *et al.*, Impairment of starvation-induced and constitutive autophagy in Atg7-deficient mice. *The Journal of cell biology* **169**, 425-434 (2005).
35. K. Kuba *et al.*, Impaired heart contractility in Apelin gene-deficient mice associated with aging and pressure overload. *Circ Res* **101**, e32-42 (2007).
36. G. F. Mitchell, A. Jeron, G. Koren, Measurement of heart rate and Q-T interval in the conscious mouse. *The American journal of physiology* **274**, H747-751 (1998).
37. Y. Nishida *et al.*, Discovery of Atg5/Atg7-independent alternative macroautophagy. *Nature* **461**, 654-658 (2009).
38. F. J. Salles, W. G. Richards, S. Strickland, Assaying the polyadenylation state of mRNAs. *Methods* **17**, 38-45 (1999).
39. M. Morita *et al.*, The lipid mediator protectin D1 inhibits influenza virus replication and improves severe influenza. *Cell* **153**, 112-125 (2013).

40. I. Gupta *et al.*, Translational Capacity of a Cell Is Determined during Transcription Elongation via the Ccr4-Not Complex. *Cell Rep* **15**, 1782-1794 (2016).
41. A. M. Bolger, M. Lohse, B. Usadel, Trimmomatic: a flexible trimmer for Illumina sequence data. *Bioinformatics* **30**, 2114-2120 (2014).
42. Y. Nakano *et al.*, HIV-1 competition experiments in humanized mice show that APOBEC3H imposes selective pressure and promotes virus adaptation. *PLoS Pathog* **13**, e1006348 (2017).
43. G. Yu, L. G. Wang, Y. Han, Q. Y. He, clusterProfiler: an R package for comparing biological themes among gene clusters. *OMICS* **16**, 284-287 (2012).
44. T. Sato *et al.*, Apelin is a positive regulator of ACE2 in failing hearts. *The Journal of clinical investigation* **123**, 5203-5211 (2013).
45. I. Tanida *et al.*, Apg7p/Cvt2p: A novel protein-activating enzyme essential for autophagy. *Mol Biol Cell* **10**, 1367-1379 (1999).
46. M. Morita *et al.*, Obesity resistance and increased hepatic expression of catabolism-related mRNAs in Cnot3+/- mice. *Embo j* **30**, 4678-4691 (2011).
47. M. Morita *et al.*, Depletion of mammalian CCR4b deadenylase triggers elevation of the p27Kip1 mRNA level and impairs cell growth. *Mol Cell Biol* **27**, 4980-4990 (2007).
48. X. Xu *et al.*, Diminished autophagy limits cardiac injury in mouse models of type 1 diabetes. *J Biol Chem* **288**, 18077-18092 (2013).

Acknowledgments: We thank all members of our laboratories for technical assistance and helpful discussions.

Funding: KK is supported by Funding Program for Next Generation World-Leading Researchers Grant Number LS015, Japan Society for the Promotion of Science (JSPS) KAKEN Grant Numbers 30733422, 16K19013, 17H04028 and JST PRESTO Grant Number JPMJPR13MD. YS is supported by Platform for Advanced Genome Sciences of JSPS KAKEN Grant Number 16H06279. SN is supported by JST PRESTO Grant Number JPMJPR16E9 and JSPS KAKEN Grant Numbers 15KT0147 and 16K05265. A.Kimura and S.Shimizu are supported by Nanken-Kyoten, Tokyo Medical and Dental University. S.Shimizu is supported by JSPS KAKEN Grant

Numbers 17H01533 and 15K19004. YI is supported by JSPS KAKEN Grant Number 17H06179.

Author contributions: K.K. and Y.I. designed the project. T.Yamaguchi, T.Suzuki, and T.Sato performed experiments with the assists of A.Kadowaki, M.N. and Y.K. K.K., H.Inagaki, A.T. and T.Yamamoto generated knockout mice. S.Arakawa and S.Shimizu performed TEM analysis. S.N. and Y.S. performed RIP-seq analysis. H.W., S.Seki, S.Adachi, A.F., T.F., T.N., M.K., A.Kimura, H.Ito, and J.M.P. provided unpublished new experimental materials. K.K. and T.Yamaguchi analyzed the data. K.K. organized the project and wrote the manuscript.

Competing interests: The authors declare that they have no competing interests.

Data and materials availability: The RIP-seq data have been deposited in NCBI's Gene Expression Omnibus (GEO, http://www.ncbi.nlm.nih.gov/geo/) under the accession number GSE103629.

Figure legends

Fig. 1. Severe heart failutre by muscle-specific deletion of Cnot3 in mice.

A, Western blot for CCR4-NOT complex subunits in the hearts of WT and Cnot3 muscle knockout mice (Cnot3 mKO), representative of 3 mice per genotype in 3 independent experiments. **B,** Postnatal survival curve for WT (n=7) and Cnot3 mKO (n=7) mice. Tissue samples were harvested at postnatal day 19 (arrow head). **C,** Macroscopic pictures and sections of the hearts of WT and Cnot3 mKO mice (representative of 3 mice per genotype). Bars indicate 1 mm. **D,** Heart weights (HW) of WT (n=7) and Cnot3 mKO (n=7) mice. BW, body weight. **E-F,** Heart function measurements of WT (n=12) Cnot3 mKO (n=9) mice. Representative M-mode echocardiography (**E**, left), left ventricular end-diastolic diameter (LVEDD), left ventricular end-systolic diameter (LVESD), %Fractional shortening (%FS) (**E**, right), representative electrocardiogram (ECG) chart (**F**, left) and QTc (corrected QT) interval (**F**, right) for WT and Cnot3 mKO mice at 19 days of age are shown. **G,** Hematoxylin & Eosin histology of hearts of WT and Cnot3 mKO mice, representative of 3 mice per genotype. Bars indicate 20 μm. **H,** Myofibrils in WT and Cnot3 mKO mouse hearts, representative of 3 mice per genotype. Myofibrils (F-actin staining, red) and nuclei (DAPI, blue) are visualized. Bars indicate 20 μm. All values are means ± SEM. *P < 0.05, **P < 0.01, unpaired two-tailed Student's *t*-tests.

Fig. 2. CCR4-NOT depletion results in severe heart failure in mice.

A, Co-immunoprecipitation of Cnot1, Cnot6l and Cnot7 with Cnot3 from the lysates of mouse hearts. N=2 independent experiments. **B,** Western Blot for Cnot1, Cnot3, Cnot6l and Cnot7 in the hearts of Cnot1 muscle knockout (Cnot1 mKO) mice. N=3 independent experiments. **C,** Postnatal survival curve for WT (n=6) and Cnot1 mKO (n=15) mice. Tissue samples were harvested at postnatal day 9 (arrow head). **D,** Macroscopic pictures of the hearts (left) and heart weights (right) of WT (n=13) and Cnot1 mKO (n=12) mice. Bars indicate 1 mm. **E,** Body weights (left) and skeletal muscle weights (right) of WT (n=11) and Cnot1 mKO (n=11) mice. Ga-MW, gastrocnemius-muscle weight. **F-G,** Heart function measurements of WT (n=12) and Cnot1 mKO (n=11) mice. Representative M-mode echocardiography (**F**, left), %Fractional shortening (%FS) (**F**, right), representative ECG chart (**G**, left) and QTc interval (**G**, right) for WT and Cnot1 mKO mice at postnatal day 9 are shown. **H,** Hematoxylin & Eosin histology of WT (representative of n=3) and Cnot1 mKO (representative of n=3) mouse hearts. Bars indicate 20 μm. All values are means ± SEM. *P < 0.05, **P < 0.01, unpaired two-tailed Student's *t*-tests.

Fig. 3. Autophagy protein abundance but not autophagy flux is altered in Cnot3-depleted heart.

A, TEM analysis for WT (representative of n=3) and Cnot3 mKO (representative of n=3) mouse hearts. Higher magnification of the colored rectangle (top) is shown in the bottom panel. Bars indicate 5 μm in top panels and 1 μm in bottom panels. **B,** Western Blot for autophagy factors in the hearts of WT and Cnot3 mKO mice under fed and fasting conditions. Representative blots (left panel and Fig. S3A) of n=3 independent

experiments are quantified for fed condition with WT (n=5) and Cnot3 mKO (n=5) mice (right top panel) and for fasting condition with WT (n=3) and Cnot3 mKO (n=3) mice (right bottom panel). **C,** Western Blot for LC3 and p62 in the hearts of WT and Cnot3 mKO mice treated with or without Bafilomycin A1 (Baf-A1). Representative blots (left panel and Fig. S3C) of n=3 independent experiments were quantified for WT mice treated with vehicle (n=7), Cnot3 mKO mice treated with vehicle (n=7), WT mice treated with Baf-A1 (n=6) and Cnot3 mKO mice treated with Baf-A1 (n=6). **D,** Immunocytochemistry of LC3 in mouse cardiomyocytes transfected with Cnot3 (si-Cnot3) or control (si-Control) siRNAs and treated with or without E64d and pepstatin A (Pep). N=2 independent experiments with two different siRNAs for Cnot3 (Fig. S3D). Bars indicate 20 μm. **E,** Western Blot for LC3 and p62 in WT and Cnot3 KO MEFs treated with or without E64d plus pepstatin A (Pep). N=2 independent experiments. All values are means ± SEM. *P < 0.05, **P < 0.01, unpaired two-tailed Student's *t*-tests.

Fig. 4. Poly(A) tail length and stability of autophagy factor-encoding mRNAs are regulated by CCR4-NOT complex.

A, RIP-seq plot of the applied cutoff to identify significantly bound or unbound mRNAs by Cnot3 in the heart. **B,** GO-enrichment analysis for Cnot3 DEGs. **C,** Autophagy factor-encoding mRNAs in Cnot3 IgG (αCnot3) RIP or control IgG RIP, normalized to input, for two biological replicates (Rep1 and Rep2). #; *Atg7* was selected as a gene enriched in Cnot3 RIP by R bioconductor package edgeR with the criteria of FDR < 0.05, cpm for mean Input > 0.1 and αCnot3 RIP/Input > $2^{0.5}$. **D,** qRT-PCR to measure the expression of autophagy factor-encoding mRNAs in the hearts of WT (n=6) and

Cnot3 mKO (n=6) mice. N=2 independent experiments. **E,** Poly(A) tail length measurements of autophagy factor-encoding mRNAs in hearts (left) and mouse cardiomyocytes (right). Total RNA was subjected to PCR-based poly(A)-tail length analysis. Representative results for the hearts of WT (n=3) and Cnot3 mKO (n=3) mice at 18 days old (left) and cardiomyocytes transfected with si-Cnot3 or siRNA combinations for Cnot6, Cnot6l, Cnot7 and Cnot8 (si-Cnot6/6l/7/8) (right). Control PCR without poly(A) regions are shown in Fig. S5E and S6E. N=3 independent experiments. **F,** The stability of autophagy factor-encoding mRNAs in cardiomyocytes was analyzed after actinomycin D treatment. N=3 independent experiments. The data obtained with a second set of siRNAs for Cnot3 and Cnot6/6l/7/8 are shown in Fig. S6A-F. All values are means ± SEM. *P < 0.05, **P < 0.01, unpaired two-tailed Student's *t*-tests.

Fig. 5. Atg7 promotes cardiac dysfunction in Cnot3 mKO mice.

A, Western Blot for autophagy proteins in the hearts. The hearts of WT, Cnot3 mKO, Cnot3;Atg7 double muscle knockout (Cnot3;Atg7 dmKO) and Cnot3;Atg5 double muscle knockout (Cnot3;Atg5 dmKO) mice at 18 days old under normal diet feeding were harvested. Gapdh was used as a loading control. N=2 independent experiments. **B,** Postnatal survival curve for WT (n=6), Cnot3 mKO (n=11), Atg7 mKO (n=5), and Cnot3;Atg7 dmKO (n=5) mice. **C,** Macroscopic images of the hearts of WT (representative of n=3), Cnot3 mKO (representative of n=3), Atg7 mKO (representative of n=3), Cnot3;Atg7 dmKO (representative of n=3) mice (left). Heart weight to body weight ratios (HW/BW) WT (n=4), Cnot3 mKO (n=4), Atg7 mKO (n=3), Cnot3;Atg7 dmKO (n=4) mice at 18 days after birth (right). Bars indicate 2 mm. **D,** Representative

M-mode echocardiography (left) and %Fractional shortening (right) at 18 days of age for WT (n=5), Cnot3 mKO (n=5), Atg7 mKO (n=3) and Cnot3;Atg7 dmKO (n=5) mice. **E,** Electrocardiogram (ECG) measurements. Representative ECG chart (left) and QTc interval (right) of WT (n=9), Cnot3 mKO (n=9), Atg7 mKO (n=3) and Cnot3;Atg7 dmKO (n=5) mice at postnatal day 18 are shown. **F,** Hematoxylin & Eosin histology of the hearts of WT (representative of n=3), Cnot3 mKO (representative of n=3), Atg7 mKO (representative of n=2), Cnot3;Atg7 dmKO (representative of n=3) mice. Bars indicate 20 μm. **G,** Myofibrils of the heart sections of Cnot3 mKO (representative of n=3) and Cnot3;Atg7 dmKO (representative of n=3) mice at 18 days of age. Myofibrils (F-actin staining, red) and nuclei (DAPI, blue) were visualized. Bars indicate 20 μm. All values are means ± SEM. *P < 0.05, **P < 0.01, unpaired two-tailed Student's *t*-tests.

Fig. 6. Atg7 promotes cardiac dysfunction in Cnot1 mKO mice.

A, qRT-PCR analysis of *Cnot1* and *Atg7* expression in the hearts of WT, Cnot1 mKO, Atg7 mKO and Cnot1;Atg7 dmKO mice at 8 days old. N=3 independent experiments. **B,** Postnatal survival of WT (n=18), Cnot1 mKO (n=18), Atg7 mKO (n=5), and Cnot1;Atg7 dmKO (n=17) mice. **C,** Representative M-mode echocardiography (left) and %Fractional shortening (right) for WT (n=13), Cnot1 mKO (n=6), Atg7 mKO (n=3), Cnot1;Atg7 dmKO (n=7) mice at 8 days old. **D,** Electrocardiogram (ECG) measurements. Representative ECG chart (left) and QTc interval (right) of WT (n=11), Cnot1 mKO (n=6), Atg7 mKO (n=3), and Cnot1;Atg7 dmKO (n=5) mice at postnatal day 8 are shown. **E,** Hematoxylin & Eosin histology of the hearts of WT (representative of n=3), Cnot1 mKO (representative of n=3) and Cnot1;Atg7 dmKO (representative of

n=3) mice. Bars indicate 50 μm. All values are means ± SEM. *P < 0.05, **P < 0.01, unpaired two-tailed Student's *t*-tests.

Fig. 7. Atg7 regulates p53 activity to induce expression of cell death-associated genes under Cnot3 depletion.

A, Western Blot for p53 in the hearts of WT and Cnot3 mKO mice. Each lane represents an individual mouse (3 independent experiments). **B,** Immunocytochemistry of Atg7 and p53 in WT and Cnot3 KO MEFs. N=3 independent experiments. Bars indicate 20 μm. **C,** Western Blot for Atg7 and p53 in the nuclear fraction of Cnot3 KO MEFs. Representative images (left) and quantification results (right) of N=6 independent experiments are shown. *P < 0.05, **P < 0.01, paired two-tailed Student's *t*-tests. **D,** Immunocytochemistry of Atg7 in mouse cardiomyocytes. Cnot3 siRNA (si-Cnot3) or control siRNA (si-Control) was transfected into cardiomyocytes, which were immunostained for Atg7. N=2 independent experiments. Bars indicate 20 μm. **E,** Co-immunoprecipitation of Atg7 and p53. Heart lysates from wild type or Cnot3 mKO mice at 18 days old were immunoprecipitated with Atg7 IgG (αAtg7) and immunoblotted for Atg7 or p53. N=2 independent experiments. **F,** Cell death assessed by PI uptake in mouse cardiomyocytes transfected with si-Cnot3 or si-Control in combination with siRNAs for Atg7 or p53. Bars indicate 50 μm. **G,** qRT-PCR for mRNA expression of cell death-associated genes in hearts. N=3 independent experiments. **H,** ChIP-qPCR for Atg7-bound promoter regions of *Puma* (left) and *Ripk3* (right) in Cnot3 KO MEFs transfected with p53 siRNA or control siRNA. N=3

independent experiments. All values are means ± SEM. *P < 0.05, **P < 0.01, unpaired two-tailed Student's *t*-tests otherwise stated.

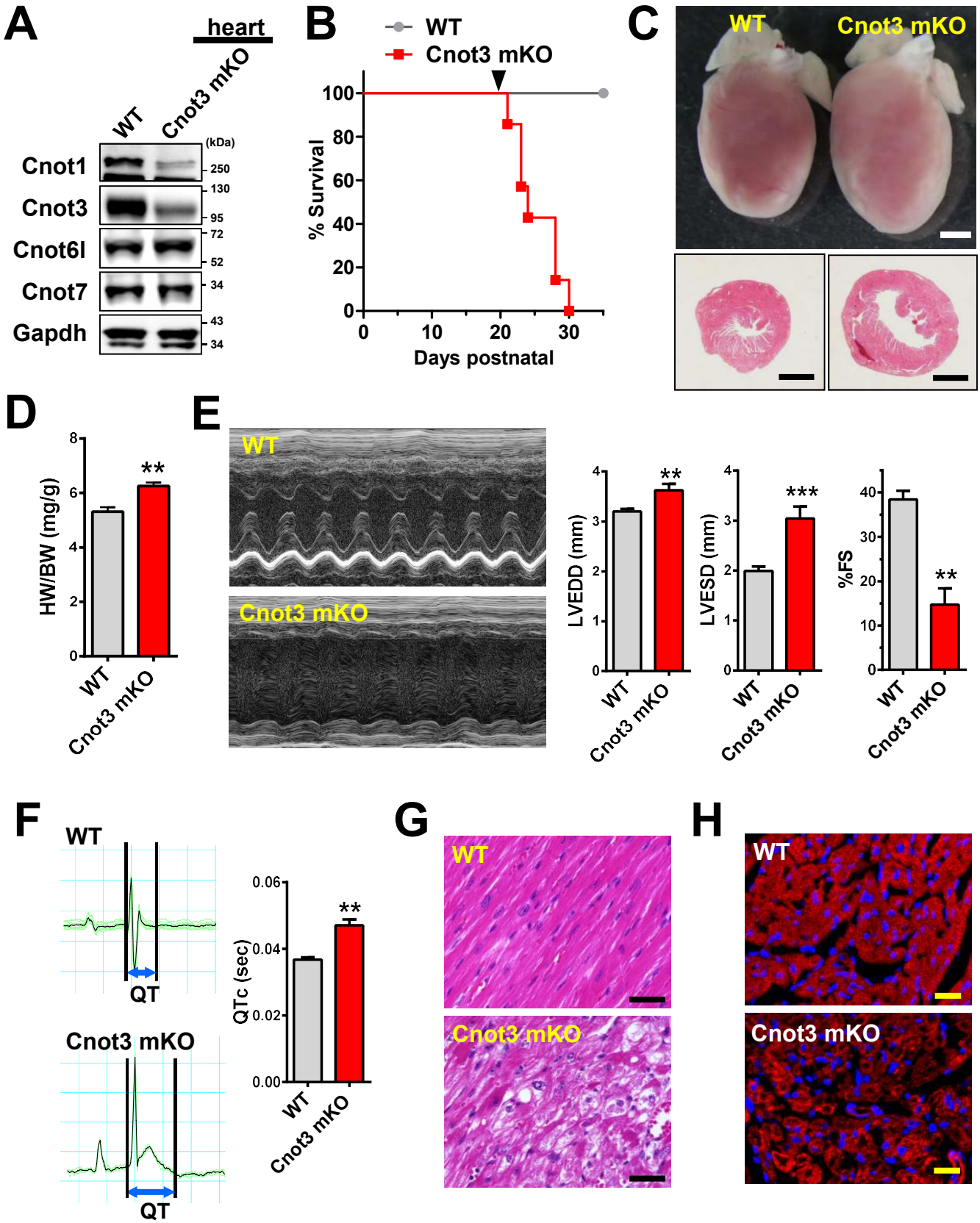
A
heart
WT
Cnot3 mKO
(kDa)
Cnot1
Cnot3
Cnot6l
Cnot7
Gapdh
250
130
95
72
52
34
43
34
B
WT
Cnot3 mKO
% Survival
Days postnatal
C
WT
Cnot3 mKO
D
HW/BW (mg/g)
E
WT
Cnot3 mKO
LVEDD (mm)
LVESD (mm)
%FS
F
WT
QT
Cnot3 mKO
QTc (sec)
G
H

Fig. 1

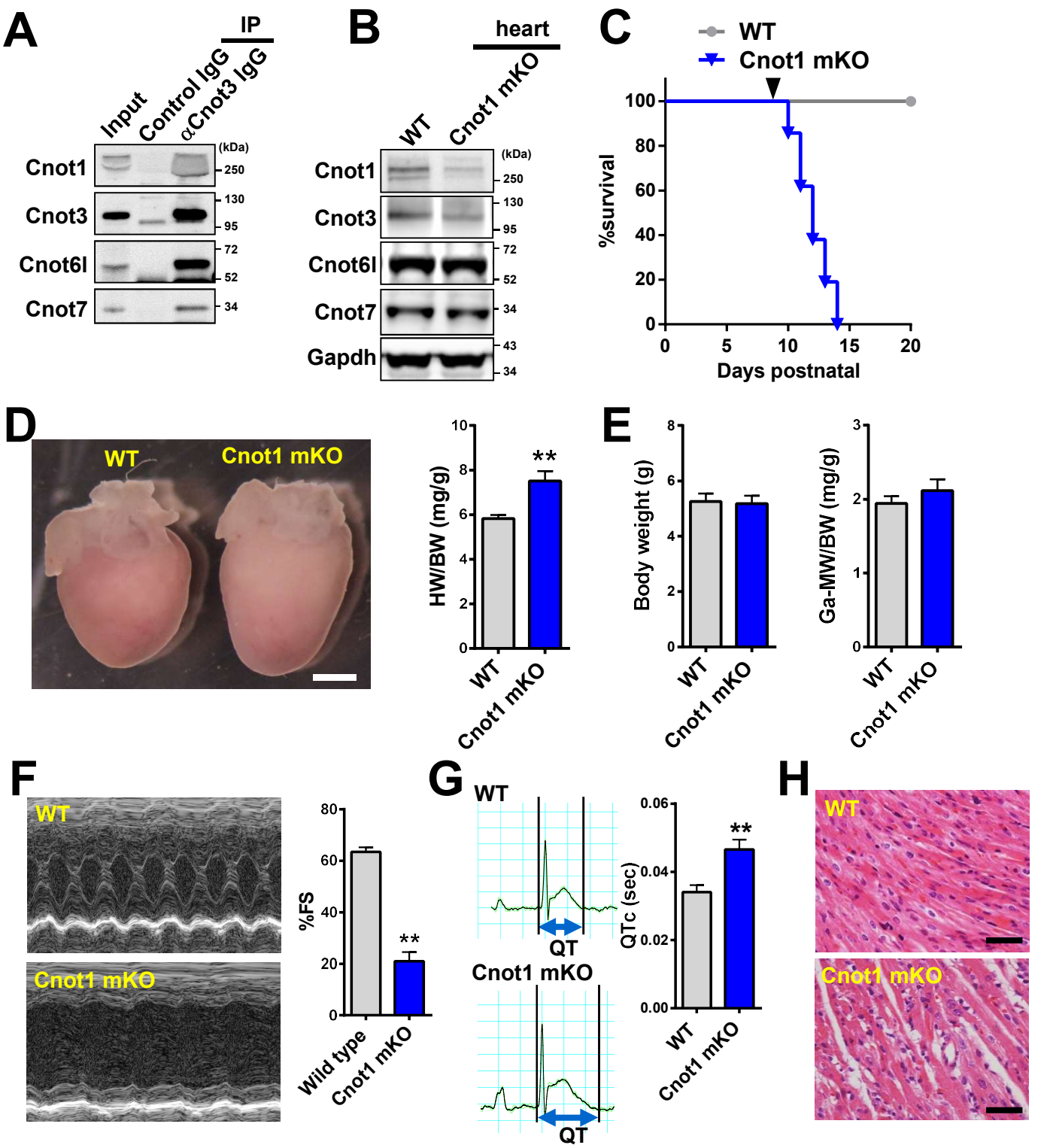
A
IP
Input
Control IgG
αCnot3 IgG
(kDa)
Cnot1
Cnot3
Cnot6l
Cnot7
250
130
95
72
52
34
B
heart
WT
Cnot1 mKO
Cnot1
Cnot3
Cnot6l
Cnot7
Gapdh
(kDa)
250
130
95
72
52
34
43
34
C
WT
Cnot1 mKO
%survival
Days postnatal
D
WT
Cnot1 mKO
HW/BW (mg/g)
**
E
Body weight (g)
Ga-MW/BW (mg/g)
F
WT
Cnot1 mKO
%FS
**
Wild type
Cnot1 mKO
G
WT
QT
Cnot1 mKO
QT
QTc (sec)
**
H
WT
Cnot1 mKO

Fig. 2

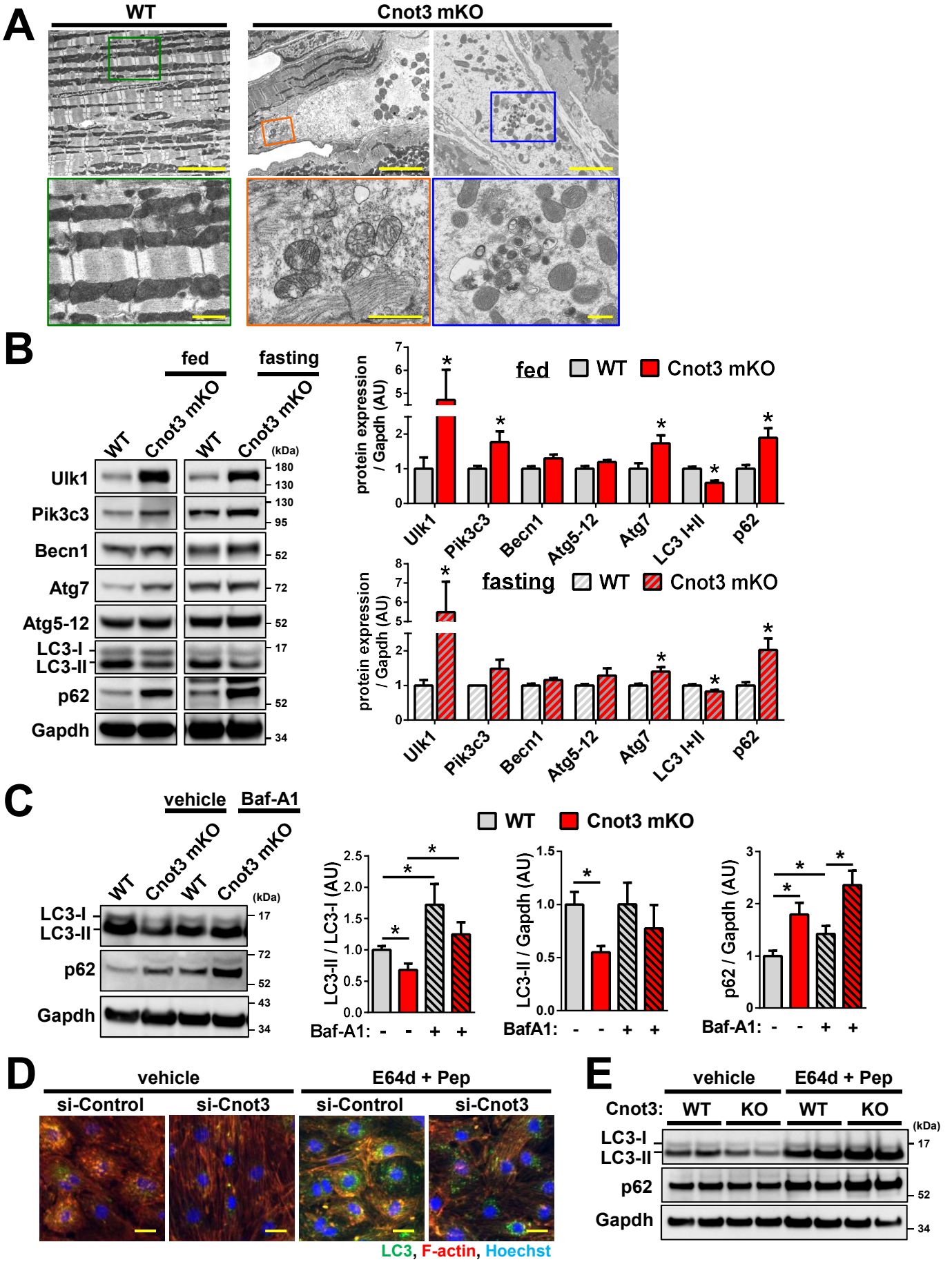
A
WT
Cnot3 mKO
B
fed
fasting
WT
Cnot3 mKO
(kDa)
Ulk1
Pik3c3
Becn1
Atg7
Atg5-12
LC3-I
LC3-II
p62
Gapdh
180
130
95
52
72
17
34
protein expression / Gapdh (AU)
Ulk1
Pik3c3
Becn1
Atg5-12
Atg7
LC3 I+II
p62
C
vehicle
Baf-A1
LC3-II / LC3-I (AU)
LC3-II / Gapdh (AU)
p62 / Gapdh (AU)
Baf-A1: - - + +
BafA1: - - + +
D
vehicle
E64d + Pep
si-Control
si-Cnot3
LC3, F-actin, Hoechst
E
Cnot3: WT KO WT KO
Fig. 3

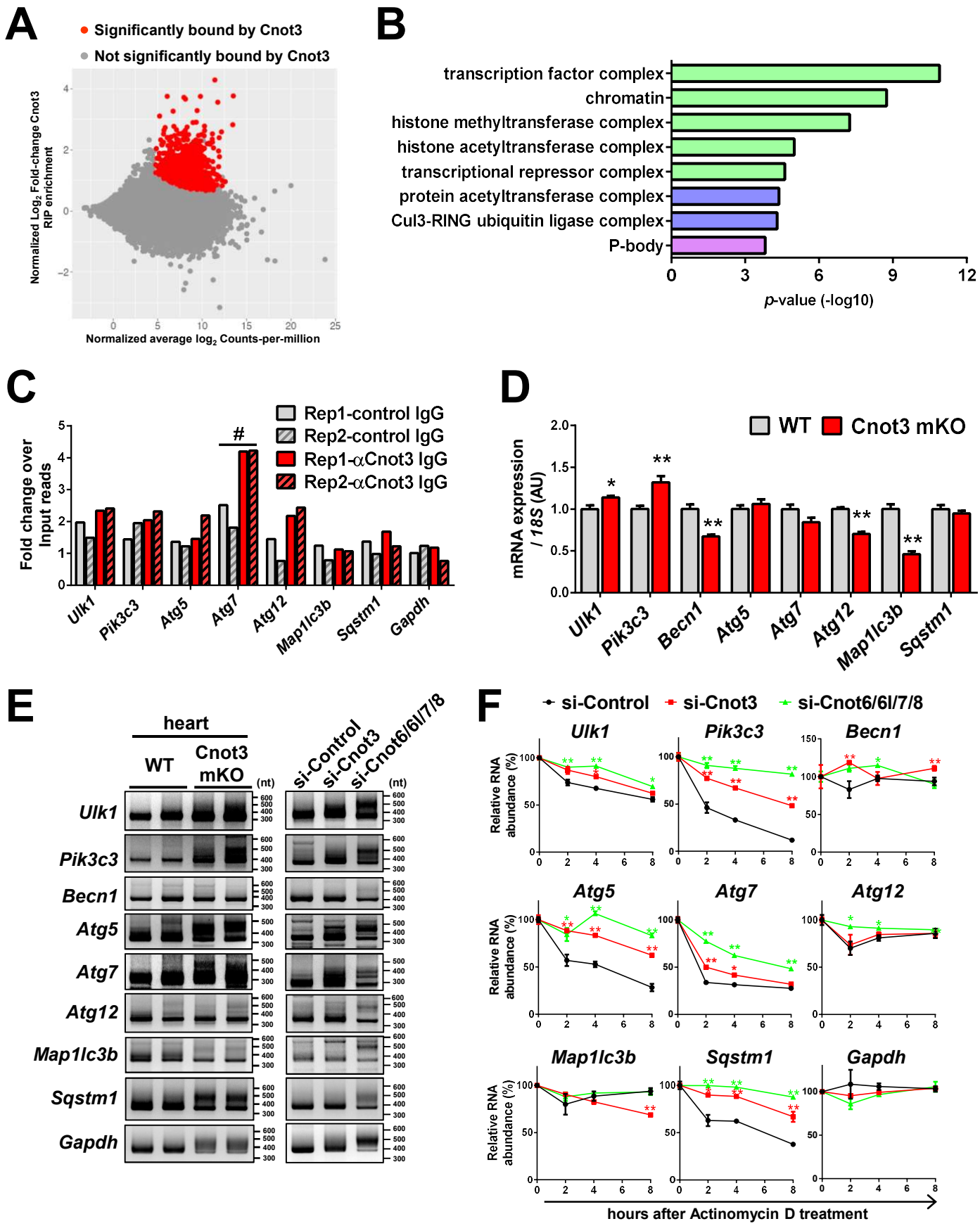
A
Significantly bound by Cnot3
Not significantly bound by Cnot3
Normalized Log2 Fold-change Cnot3 RIP enrichment
Normalized average log2 Counts-per-million
B
transcription factor complex
chromatin
histone methyltransferase complex
histone acetyltransferase complex
transcriptional repressor complex
protein acetyltransferase complex
Cul3-RING ubiquitin ligase complex
P-body
p-value (-log10)
C
Rep1-control IgG
Rep2-control IgG
Rep1-αCnot3 IgG
Rep2-αCnot3 IgG
Fold change over Input reads
Ulk1
Pik3c3
Atg5
Atg7
Atg12
Map1lc3b
Sqstm1
Gapdh
D
WT
Cnot3 mKO
mRNA expression / 18S (AU)
Ulk1
Pik3c3
Becn1
Atg5
Atg7
Atg12
Map1lc3b
Sqstm1
E
heart
WT
Cnot3 mKO
si-Control
si-Cnot3
si-Cnot6/6l/7/8
(nt)
Ulk1
Pik3c3
Becn1
Atg5
Atg7
Atg12
Map1lc3b
Sqstm1
Gapdh
F
si-Control
si-Cnot3
si-Cnot6/6l/7/8
Relative RNA abundance (%)
hours after Actinomycin D treatment

Fig. 4

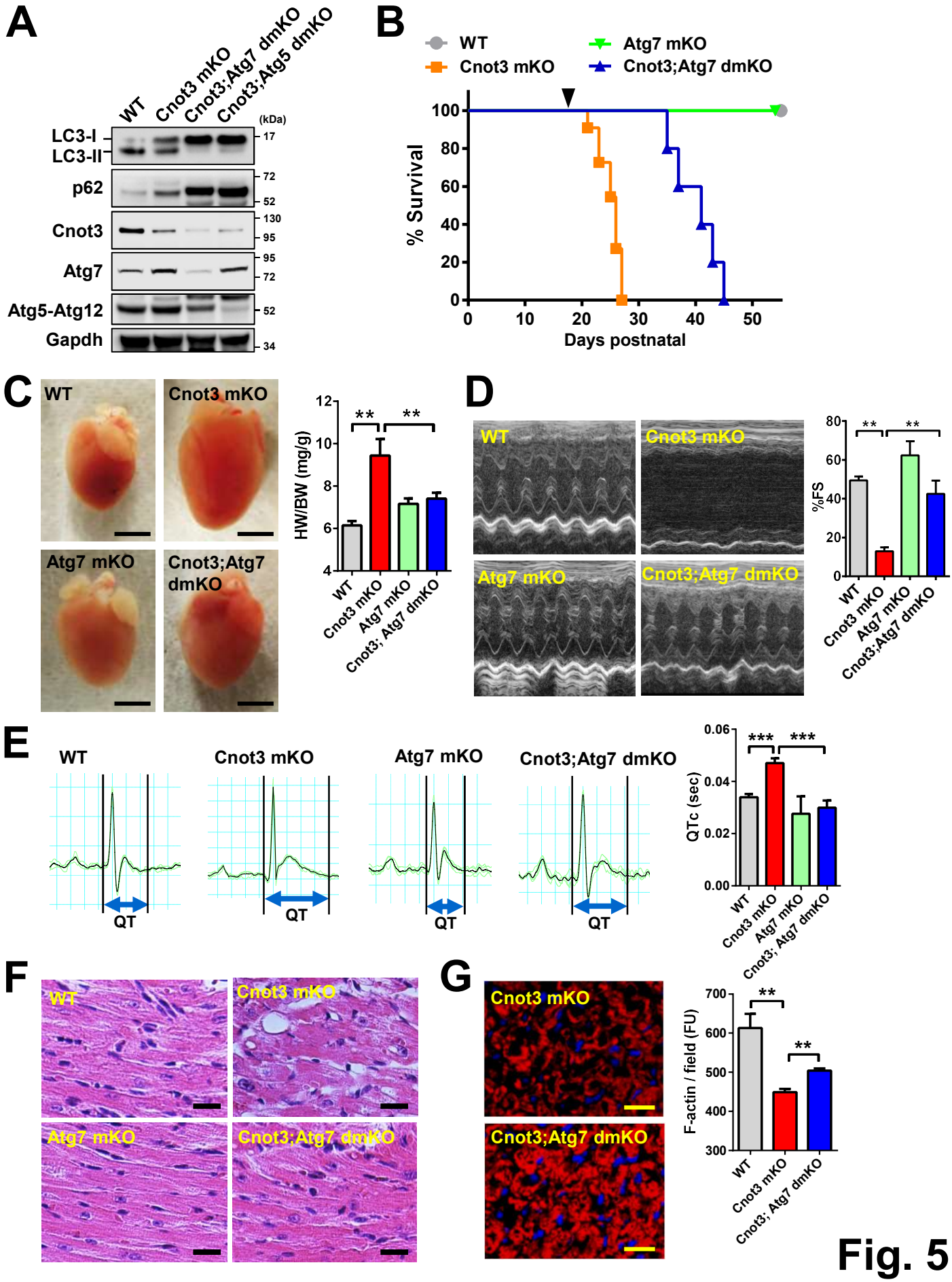
A
WT
Cnot3 mKO
Cnot3;Atg7 dmKO
Cnot3;Atg5 dmKO
(kDa)
LC3-I
LC3-II
17
p62
72
52
Cnot3
130
95
Atg7
95
72
Atg5-Atg12
52
Gapdh
34
B
WT
Cnot3 mKO
Atg7 mKO
Cnot3;Atg7 dmKO
% Survival
Days postnatal
C
WT
Cnot3 mKO
Atg7 mKO
Cnot3;Atg7 dmKO
HW/BW (mg/g)
D
%FS
E
QT
QTc (sec)
F
F-actin / field (FU)
G
Fig. 5

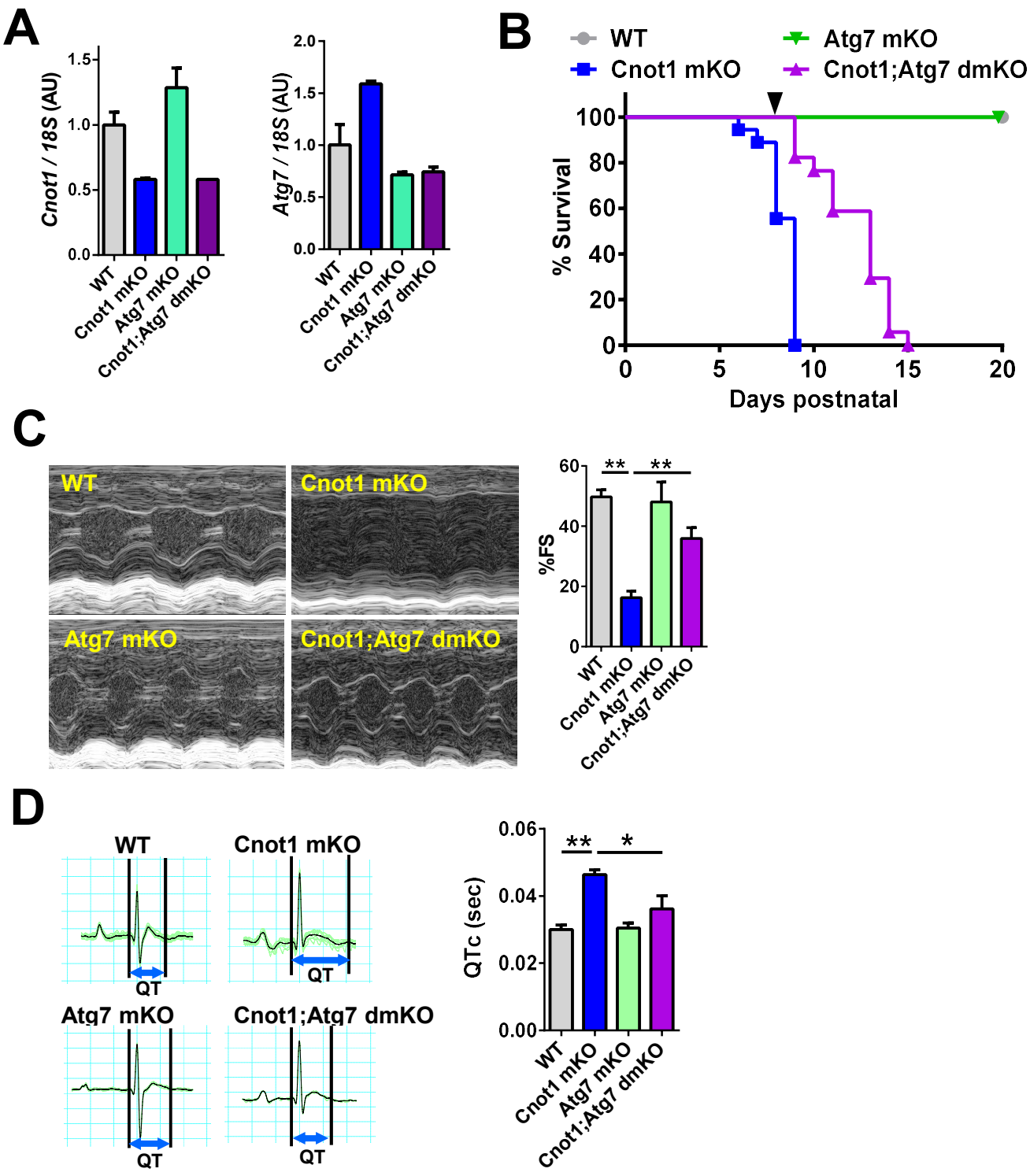
A
Cnot1 / 18S (AU)
1.5
1.0
0.5
0.0
WT
Cnot1 mKO
Atg7 mKO
Cnot1;Atg7 dmKO
Atg7 / 18S (AU)
2.0
1.5
1.0
0.5
0.0
B
WT
Cnot1 mKO
Atg7 mKO
Cnot1;Atg7 dmKO
% Survival
100
80
60
40
20
0
0
5
10
15
20
Days postnatal
C
WT
Cnot1 mKO
Atg7 mKO
Cnot1;Atg7 dmKO
%FS
60
40
20
0
**
**
D
WT
Cnot1 mKO
QT
Atg7 mKO
Cnot1;Atg7 dmKO
QTc (sec)
0.06
0.04
0.02
0.00
**
*
E
WT
Cnot1 mKO
Cnot1;Atg7 dmKO

Fig. 6

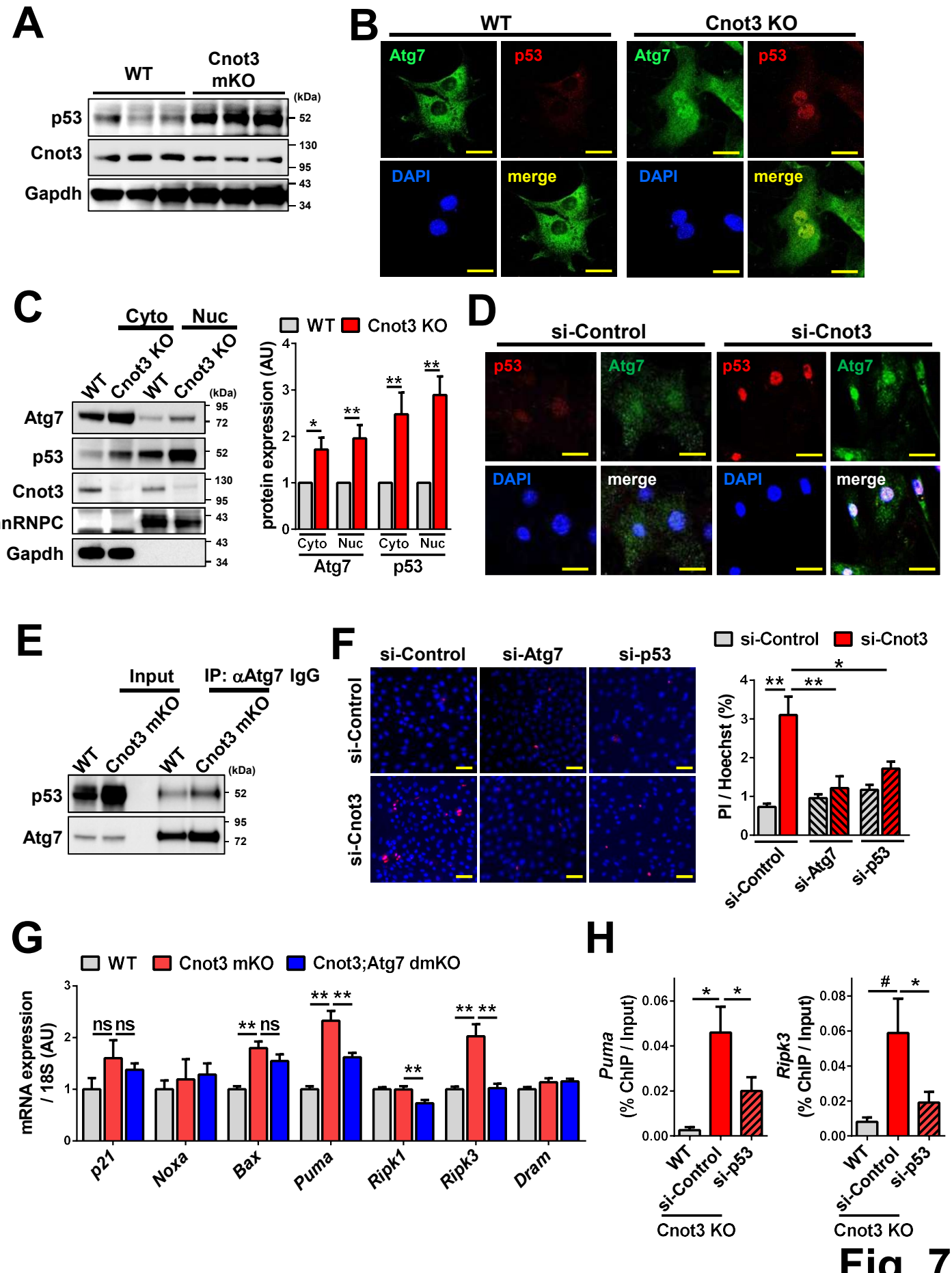
A
WT
Cnot3 mKO
(kDa)
p53
Cnot3
Gapdh
52
130
95
43
34
B
WT
Cnot3 KO
Atg7
p53
DAPI
merge
C
Cyto
Nuc
WT
Cnot3 KO
Atg7
p53
Cnot3
hnRNPC
Gapdh
protein expression (AU)
Cyto
Nuc
D
si-Control
si-Cnot3
E
Input
IP: αAtg7 IgG
F
si-Control
si-Atg7
si-p53
si-Cnot3
PI / Hoechst (%)
G
WT
Cnot3 mKO
Cnot3;Atg7 dmKO
mRNA expression / 18S (AU)
ns
p21
Noxa
Bax
Puma
Ripk1
Ripk3
Dram
H
Puma (% ChIP / Input)
Ripk3 (% ChIP / Input)
Cnot3 KO

Fig. 7

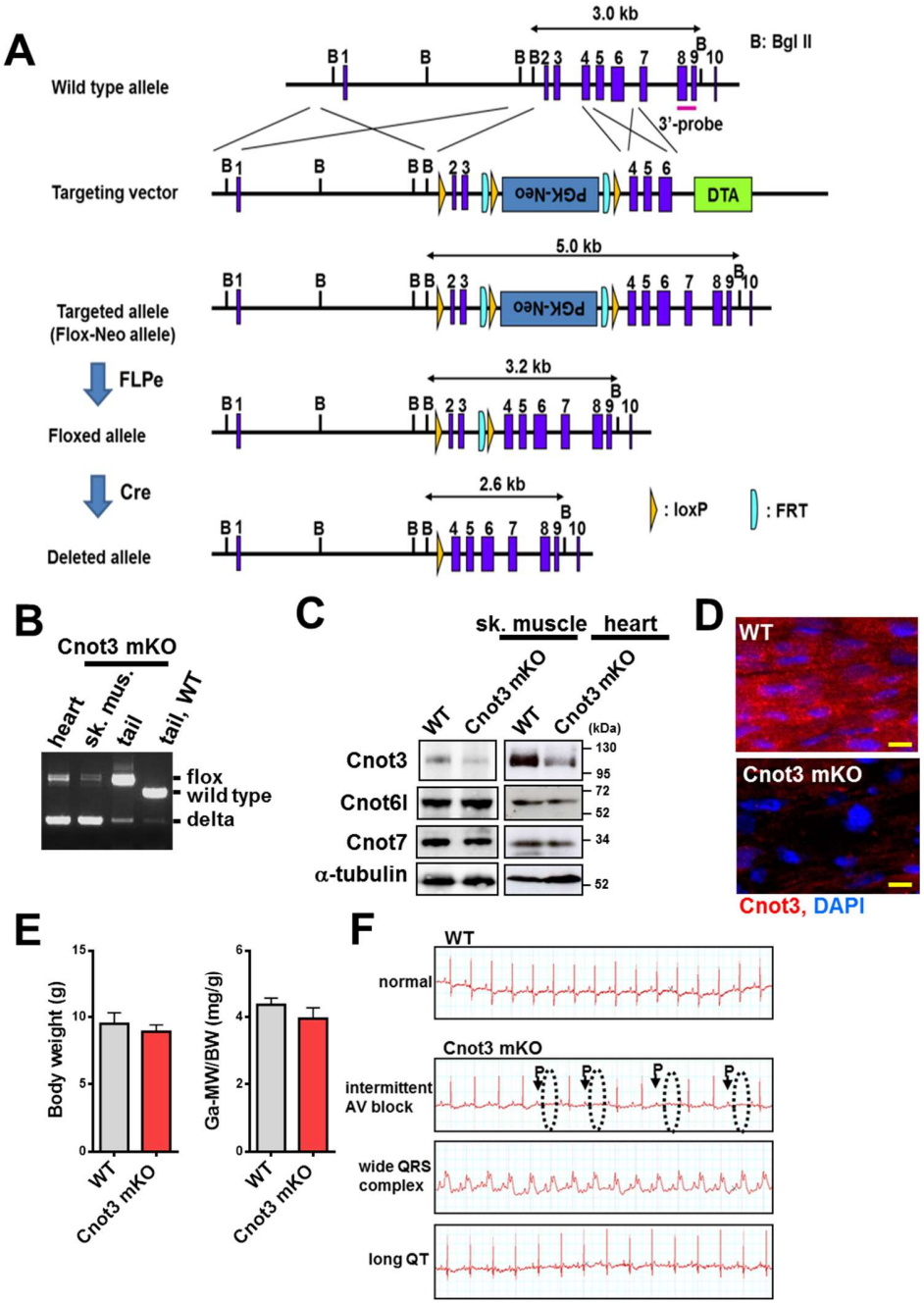

Fig. S1. Generation of Cnot3 muscle knockout (Cnot3 mKO) mice.

A, Gene targeting strategy. Exons 2 and 3 of the *Cnot3* gene were floxed with a PGK-Neo cassette by homologous recombination in A9 ES cells, which were injected into blastocysts to generate chimeric mice. The Neo cassette was removed by crossing with FLPe recombinase transgenic mice, and muscle-specific deletion of *Cnot3* was achieved by crossing with muscle creatine kinase-promoter Cre transgenic mice. The WT allele, the targeting vector, floxed allele, deleted allele, and the PGK-Neo and DTA

selection cassettes are shown. Blue boxes indicate exons. **B,** Genotyping PCR of Cnot3 muscle knockout mice (Cnot3 mKO). Deleted alleles were detected in the heart and skeletal muscle (sk. mus.) but not in the tail of Cnot3 mKO mice. **C,** Western blot for Cnot3, Cnot6l and Cnot7 in the heart and skeletal muscle of WT and Cnot3 mKO mice. N=3 independent experiments. **D,** Immunohistochemistry for Cnot3 in the hearts of WT (representative of N=3) and Cnot3 mKO (representative of N=3) mice. Bars indicate 10 μm. **E,** Body weight (left) and skeletal muscle weight (right) of WT (N=7) and Cnot3 mKO (N=7) mice. **F,** Electrocardiograms (ECGs) in WT and Cnot3 mKO mice. All values are means ± SEM.

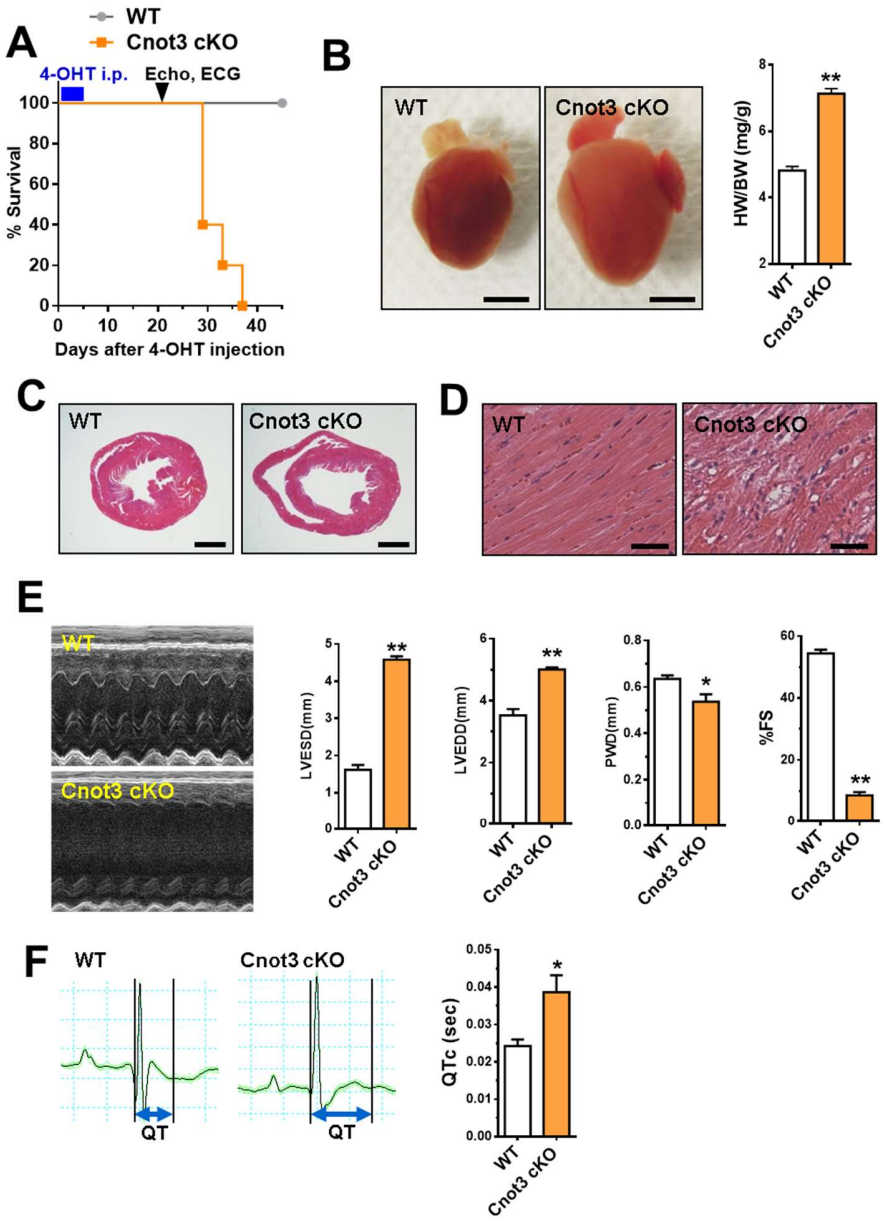

Fig. S2. Inducible cardiac-specific deletion of Cnot3 in adult mice (Cnot3 cKO).

A, Survival of WT (N=5) and cardiac inducible Cnot3 knockout (Cnot3 cKO) (N=5) mice. Cardiac deletion of Cnot3 was induced by injecting 4-hydoxytamoxifen (4-OHT; 40 mg/kg/day intraperitoneally) to *Cnot3* flox mice with the *αMHC-MerCreMer* transgene for 5 consecutive days. Measurements of echocardiography and ECG were done at 21 days after starting 4-OHT injection (arrow head). **B,** Macroscopic pictures and heart weights of WT (N=4) and Cnot3 cKO (N=3) mice. Bars indicate 2 mm. **C-D,** Hematoxylin Eosin histology of the hearts of WT (representative of N=3) and Cnot3

cKO (representative of N=3) mice. Bars indicate 1 mm in (**C**) and 20 μm in (**D**). **E-F,** Heart function measurements of WT (N=4) and Cnot3 cKO (N=3) mice. Echocardiography (**E**) and ECG (**F**) are shown. All values are means ± SEM. *P < 0.05, **P < 0.01. P values were calculated using unpaired two-tailed Student's *t*-tests.

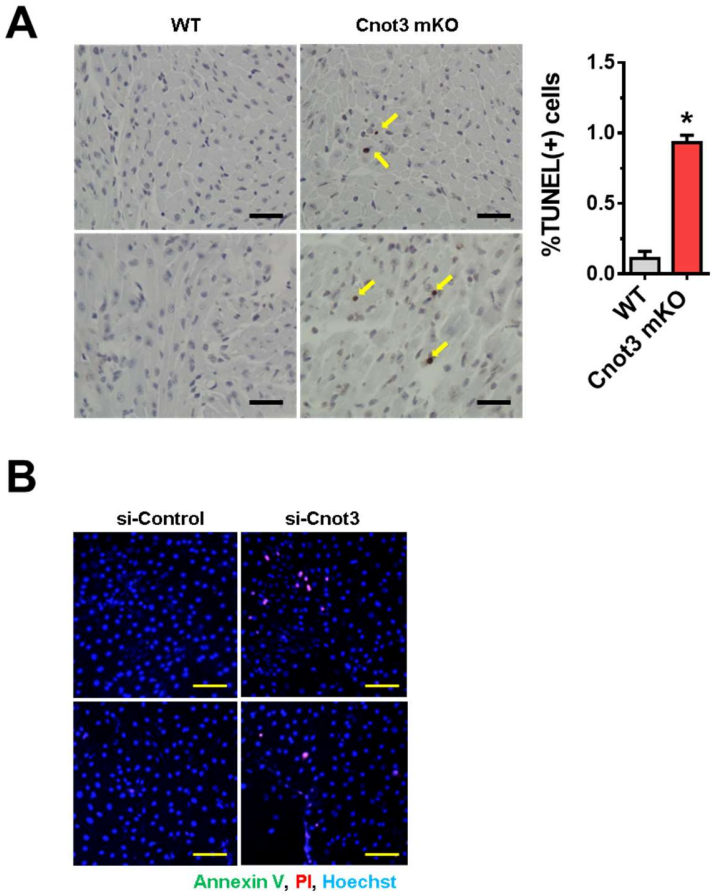

Fig. S3. Cnot3 depletion increased apoptosis and necrosis in mouse cardiomyocytes.

A, TUNEL staining of the hearts of WT (representative of N=3) and Cnot3 mKO (representative of N=3) mice. The ratio of apoptotic cells (arrows in left) to live cells are shown (right). Bars indicate 30 μm. **B,** Immunocytochemistry for annexin V and propidium iodide (PI) uptake in mouse cardiomyocytes transfected with siRNAs for Cnot3 (si-Cnot3) or non-targeted control (si-Control). N=2 independent experiments. Bars indicate 100 μm. All values are means ± SEM. *P < 0.05. P values were calculated using unpaired two-tailed Student's *t*-tests.

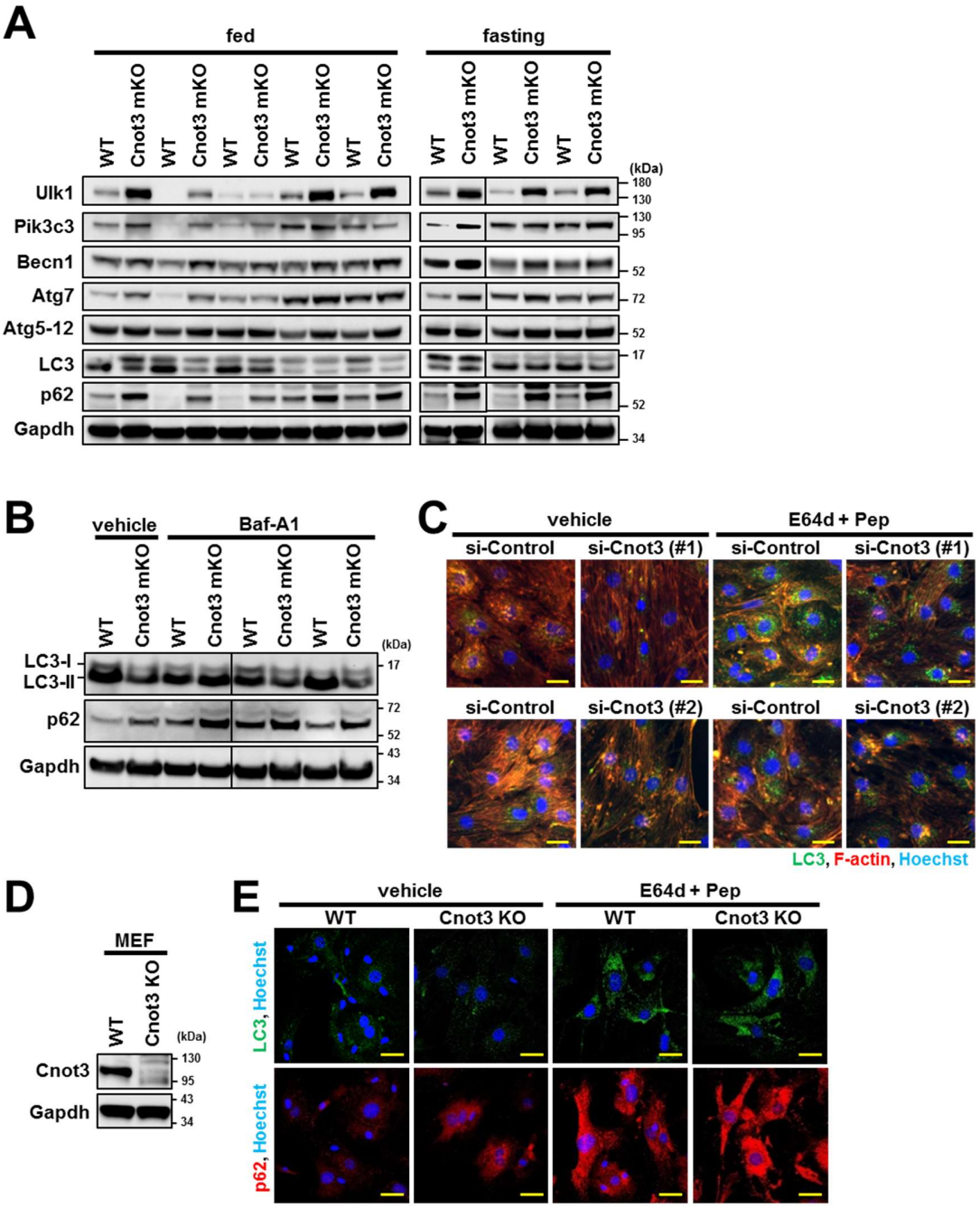

Fig. S4. Cnot3 depletion altered autophagy protein abundance without changing autophagy flux.

A, Western Blot for autophagy proteins in the hearts of fed WT (N=5) and Cnot3 mKO (N=5) mice (left panel) and the hearts of fasted WT (N=3) and Cnot3 mKO (N=3) mice (right panel). **B,** Western Blot for LC3 and p62 in the hearts of WT (N=3) and Cnot3 mKO mice (N=3) treated with or without Bafilomycin A1 (Baf-A1). **C,**

Immunocytochemistry of LC3 in mouse cardiomyocytes transfected with siRNAs for Cnot3 (si-Cnot3) or control (si-Control) and treated with or without E64d and pepstatin A (Pep). N=2 independent experiments with two different siRNAs for Cnot3. Bars indicate 20 μm. **D,** Western blot for Cnot3 in WT and Cnot3 KO MEFs. N=3 independent experiments. **E,** Immunocytochemistry for LC3 and p62 in WT and Cnot3 KO MEFs with or without E64d and pepstatin A (Pep) treatment. N=2 independent experiments. Bars indicate 20 μm.

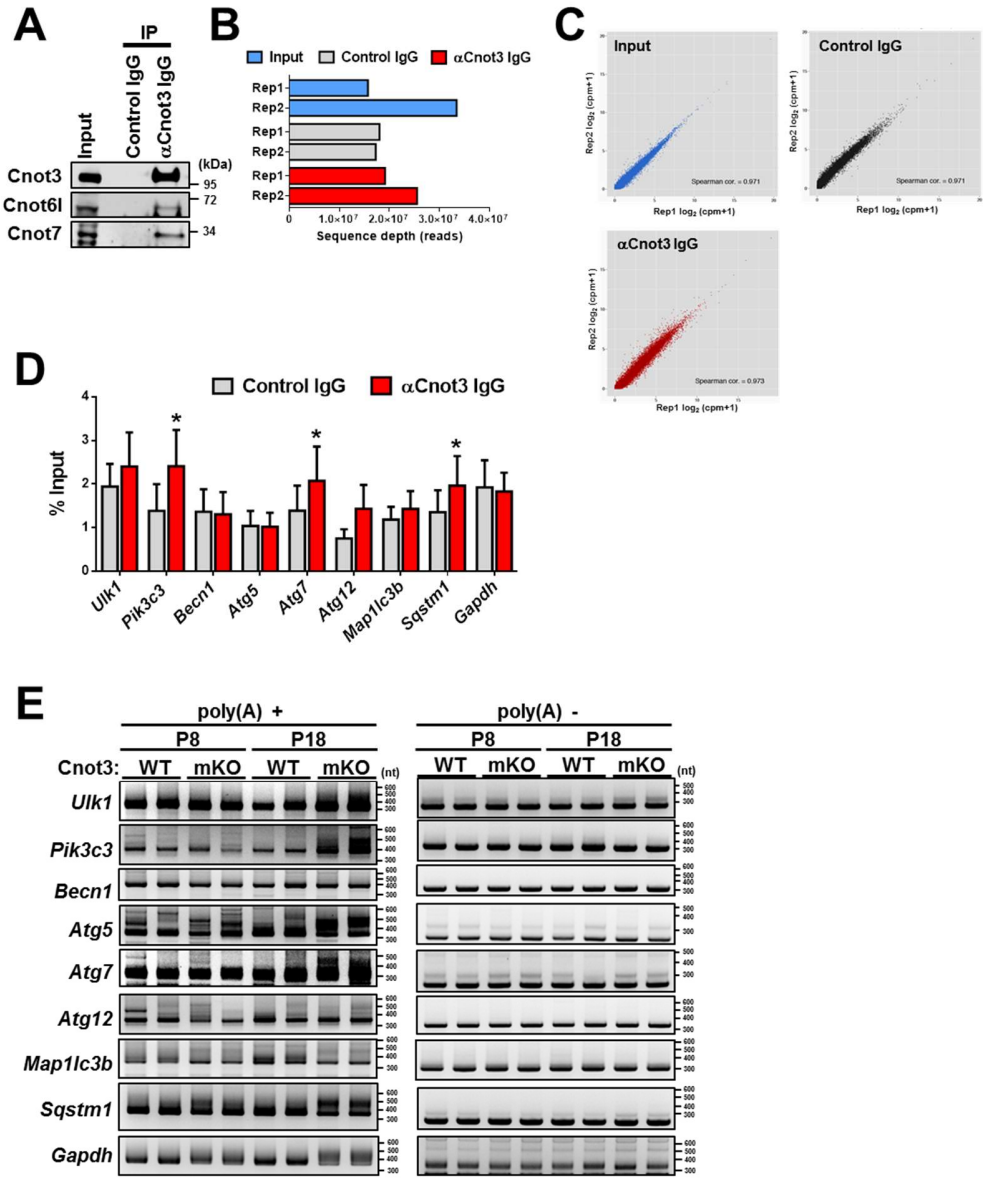

Fig. S5. Cnot3 RIP-seq analysis and poly(A) tail length measurements of autophagy factor-encoding mRNAs in hearts.

A, Co-immunoprecipitation of Cnot3 with Cnot6l and Cnot7. Cnot3 was immunoprecipitated from heart lysates from WT mice at 5 weeks old. Immunoprecipitates were immunoblotted for Cnot3, Cnot6l, or Cnot7. N=2 independent experiments. **B,** Bar plots of raw read counts for biological replicates of input, Control IgG RIP, and αCnot3 RIP. **C,** Scatterplot for the number of reads counts per gene-per million (cpm) between the each replicate of input, Control IgG RIP and αCnot3 RIP. **D,** qRT-PCR to measure the expression of autophagy factor-encoding mRNAs in control IgG RIP (N=3) and αCnot3 RIP (N=3). *P < 0.05, one-tailed paired

Student's *t*-test. **E,** Poly(A) tail length measurements of autophagy factor-encoding mRNAs in the hearts. WT and Cnot3 mKO mice at 8 days old (P8) and 18 days old (P18) were used. PCR with poly(A) regions (left) and control PCR without poly (A) regions (right) are shown. All values are means ± SEM. *P < 0.05, unpaired two-tailed Student's *t*-tests otherwise mentioned.

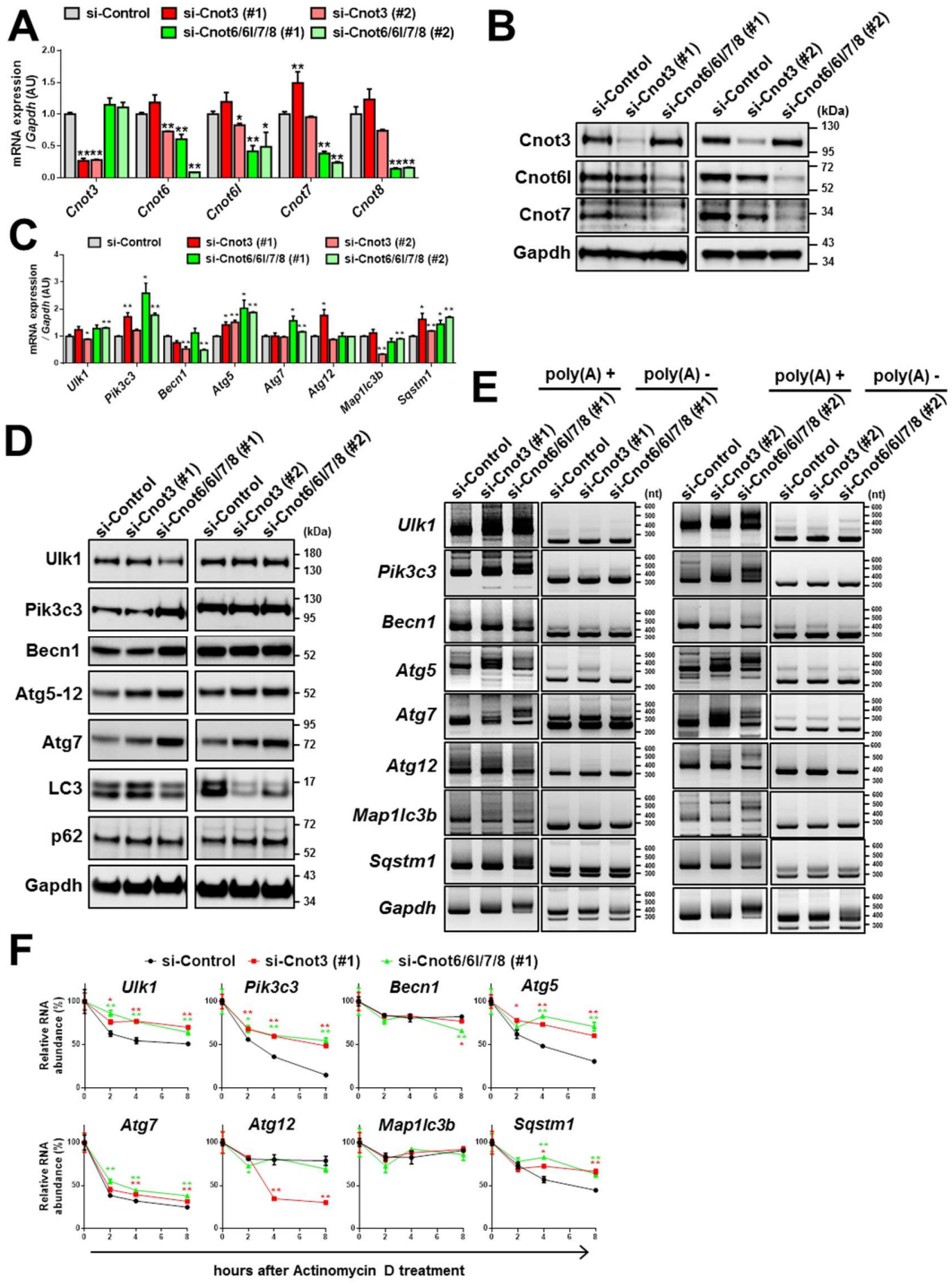

Fig. S6. Poly(A) tail length and stability of autophagy factor-encoding mRNAs are regulated by CCR4-NOT complex in cardiomyocytes.

A-D, The expression of the indicated mRNAs or proteins was measured in mouse cardiomyocytes transfected with siRNAs for control, Cnot3 (si-Cnot3) or combinations of Cnot6, Cnot6l, Cnot7 and Cnot8 siRNAs (si-Cnot6/6l/7/8). N=3 independent experiments with two different siRNAs for each gene. The results of qRT-PCR (**A**) and Western blot (**B**) analyses for the CCR4-NOT complex components are shown, and qRT-PCR (**C**) and Western blot (**D**) analyses for autophagy factors are shown. **E,** Poly(A) tail length measurements of autophagy factor-encoding mRNAs. PCR amplifying poly(A) regions (left) and control PCR for 3' UTR region without poly (A) (right) are shown. N=2 independent experiments. **F,** The stability of autophagy factor-encoding genes in cardiomyocytes was analyzed after actinomycin D treatment. N=3 independent experiments. The results of si-Cnot3(#2) and si-Cnot6/6l/7/8(#2) are shown in Fig. 4F. All values are means ± SEM. *P < 0.05, **P < 0.01. P values were calculated using unpaired two-tailed Student's *t*-tests.

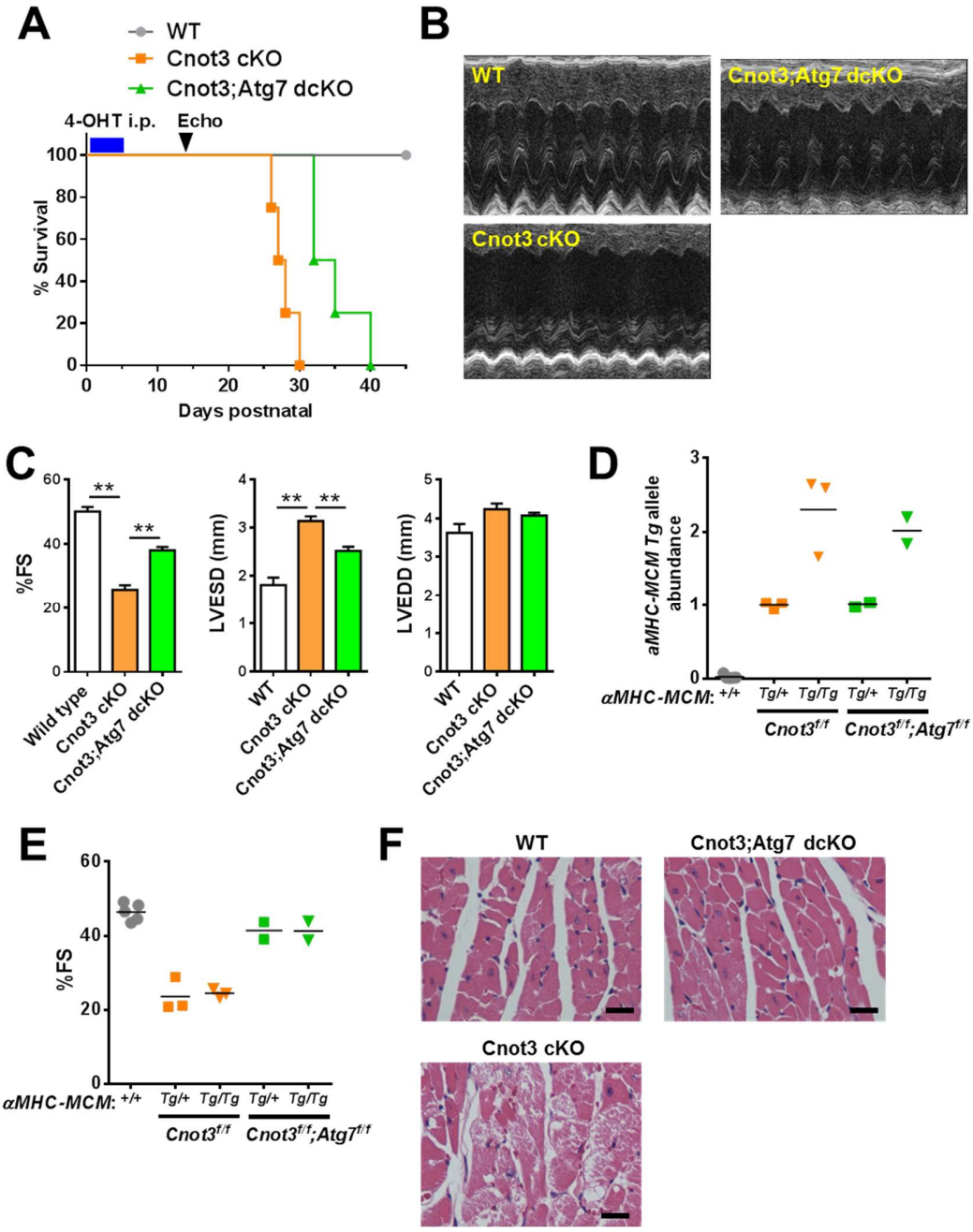

Fig. S7. Atg7 promotes cardiac dysfunction in adult Cnot3 cKO mice.
A, Survival of WT (N=4), cardiac inducible Cnot3 knockout (Cnot3 cKO) (N=4) and Cnot3;Atg7 double cardiac knockout (Cnot3;Atg7 dcKO) (N=4) mice. Cardiac deletion of Cnot3 and Atg7 was induced by injecting 4-hydoxytamoxifen (4-OHT; 40 mg/kg/day intraperitoneally) into these mice for 5 consecutive days. Measurements of echocardiography was done at 14 days after starting 4-OHT injection (arrow head). **B-**

C, Heart function measurements of WT (N=4), Cnot3 cKO (N=3), and Cnot3;Atg7 dcKO (N=5) mice. Representative M-mode echocardiography (**B**), left ventricular end-diastolic diameter (LVEDD), left ventricular end-systolic diameter (LVESD), %Fractional shortening (%FS) (**C**) are shown. **D,** qPCR analysis for allele frequency of *αMHC-MerCreMer* Tg in Cnot3 cKO and Cnot3;Atg7 dcKO hearts. *Cnot3$^{f/f}$;αMHC-MerCreMer$^{+/+}$* or *Cnot3$^{f/f}$;Atg7$^{f/f}$;αMHC-MerCreMer$^{+/+}$* (N=5), *Cnot3$^{f/f}$;αMHC-MerCreMer$^{Tg/+}$* (N=3), *Cnot3$^{f/f}$;αMHC-MerCreMer$^{Tg/Tg}$* (N=3), *Cnot3$^{f/f}$;Atg7$^{f/f}$;αMHC-MerCreMer$^{Tg/+}$* (N=2), *Cnot3$^{f/f}$;Atg7$^{f/f}$;αMHC-MerCreMer$^{Tg/Tg}$* (N=2). **E,** Heart function measurements (%Fractional shortening (%FS)) of the mice genotyped in (**D**). **F,** Hematoxylin & Eosin histology of WT, Cnot3 cKO, and Cnot3;Atg7 dcKO mouse hearts. Bars indicate 20 μm. N=2 independent experiments. All values are means ± SEM. *P < 0.05, **P < 0.01. P values were calculated using unpaired two-tailed Student's *t*-tests.

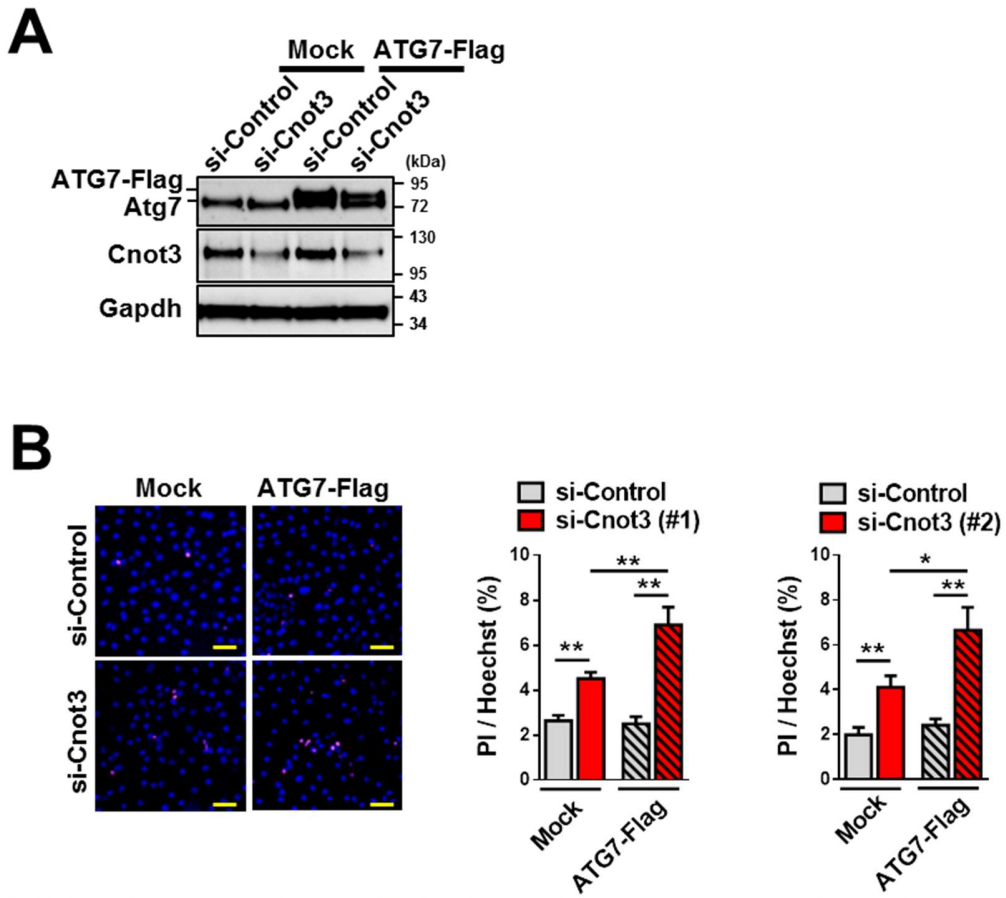

Fig. S8. Atg7 promotes cell death in Cnot3-depleted cardiomyocytes.
A, Western blot for Atg7 in mouse cardiomyocytes transfected with si-Cnot3 or si-Control in combination with control plasmid (Mock) or pCMV-hATG7 (ATG7-Flag). N=3 independent experiments. **B,** Cell death assessed by propidium iodide (PI) uptake in mouse cardiomyocytes transfected with si-Cnot3 or si-Control in combination with Mock or ATG7-Flag plasmids. N=3 independent experiments. Bars indicate 50 μm. All values are means ± SEM. *P < 0.05, **P < 0.01. P values were calculated using unpaired two-tailed Student's *t*-tests.

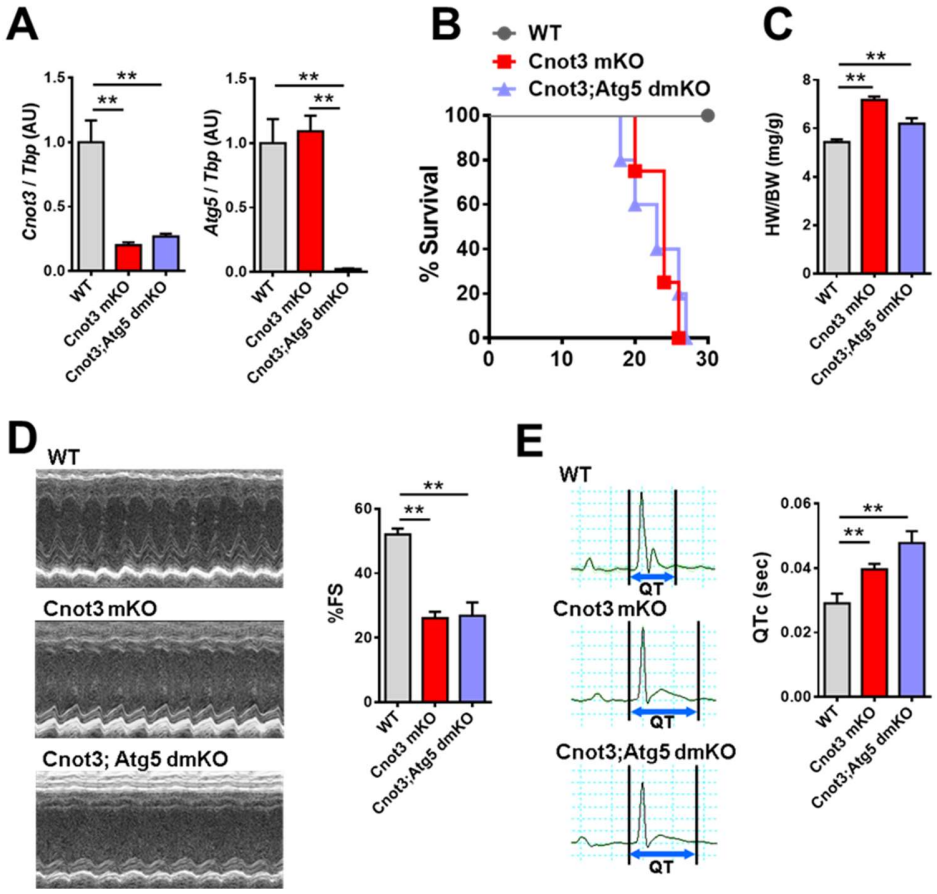

Fig. S9. No phenotypic rescue of Cnot3 mKO mice by double knockout of Cnot3 and Atg5.

A, qRT-PCR for *Cnot3* and *Atg5* expression in the hearts of WT (N=12), Cnot3 mKO (N=4) and Cnot3;Atg5 double muscle knockout (Cnot3;Atg5 dmKO) (N=4) mice. **B,** Postnatal survival of WT (N=5), Cnot3 mKO (N=4) and Cnot3;Atg5 dmKO (N=5) mice. **C,** Heart weight (HW/BW) of WT (N=13), Cnot3 mKO (N=9) and Cnot3;Atg5 dmKO (N=3) mice at postnatal day 18. **D-E,** Heart function measurements. Representative M-mode echocardiography (**D**, left), %Fractional shortening (%FS) (**D**, right), representative ECG chart (**E**, left) and QTc interval (**E**, right) for WT (N=6), Cnot3 mKO (N=4) and Cnot3;Atg5 dmKO (N=6) mice at 18 days old are shown. All values are means ± SEM. **P < 0.01. P values were calculated using unpaired two-tailed Student's *t*-tests.

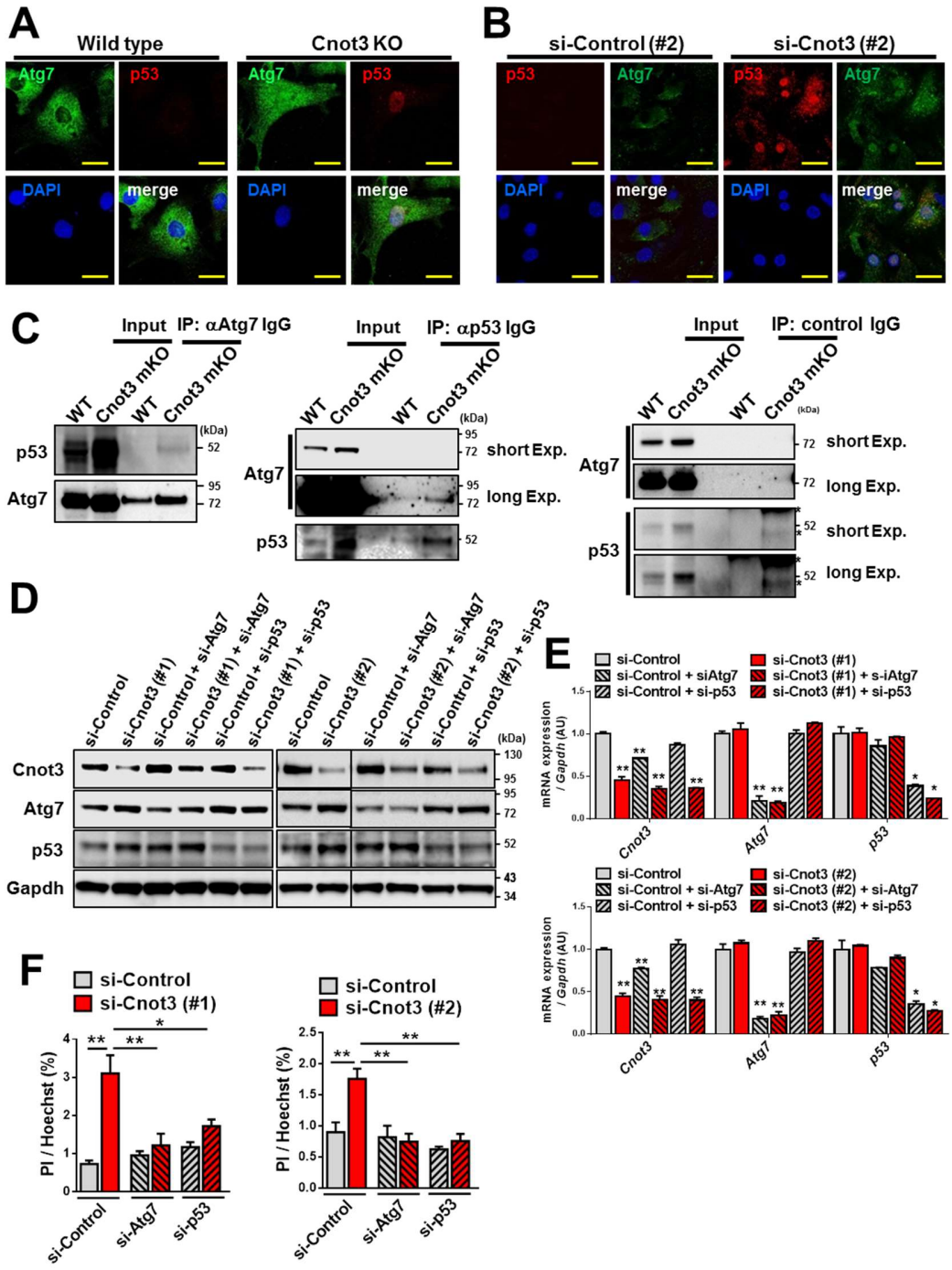

Fig. S10. Cnot3 depletion enhances the interaction of Atg7 with p53 to induce the expression of cell death-associated genes.

A, Immunocytochemistry for Atg7 and p53 in WT and Cnot3 KO MEFs. N=3 independent experiments. Bars indicate 20 μm. **B,** Immunocytochemistry for Atg7 and p53 in mouse cardiomyocytes transfected with Cnot3 siRNA (si-Cnot3) or control

siRNA (si-Control). N=2 independent experiments. Bars indicate 20 μm. **C,** Co-immunoprecipitation of Atg7 and p53. Atg7 or p53 was immunoprecipitated from heart lysates from wild type or Cnot3 mKO mice at 18 days old. Immunoprecipitates were immunoblotted for Atg7 or p53. Exposures were performed within 1 min (short Exp.) to 20 min (long Exp.). Nonspecific bands are indicated as asterisks. N=2 independent experiments. **D-E,** Western blot (**D**) and qRT-PCR (**E**) analyses for Cnot3, Atg7 and p53 in cardiomyocytes transfected with si-Cnot3 or si-Control in combination with siRNAs for Atg7 or p53. N=3 independent experiments. **F,** Cell death measurements with propidium iodide (PI) uptake in cardiomyocytes. N=3 independent experiments. All values are means ± SEM. *P < 0.05, **P < 0.01, unpaired two-tailed Student's *t*-tests.

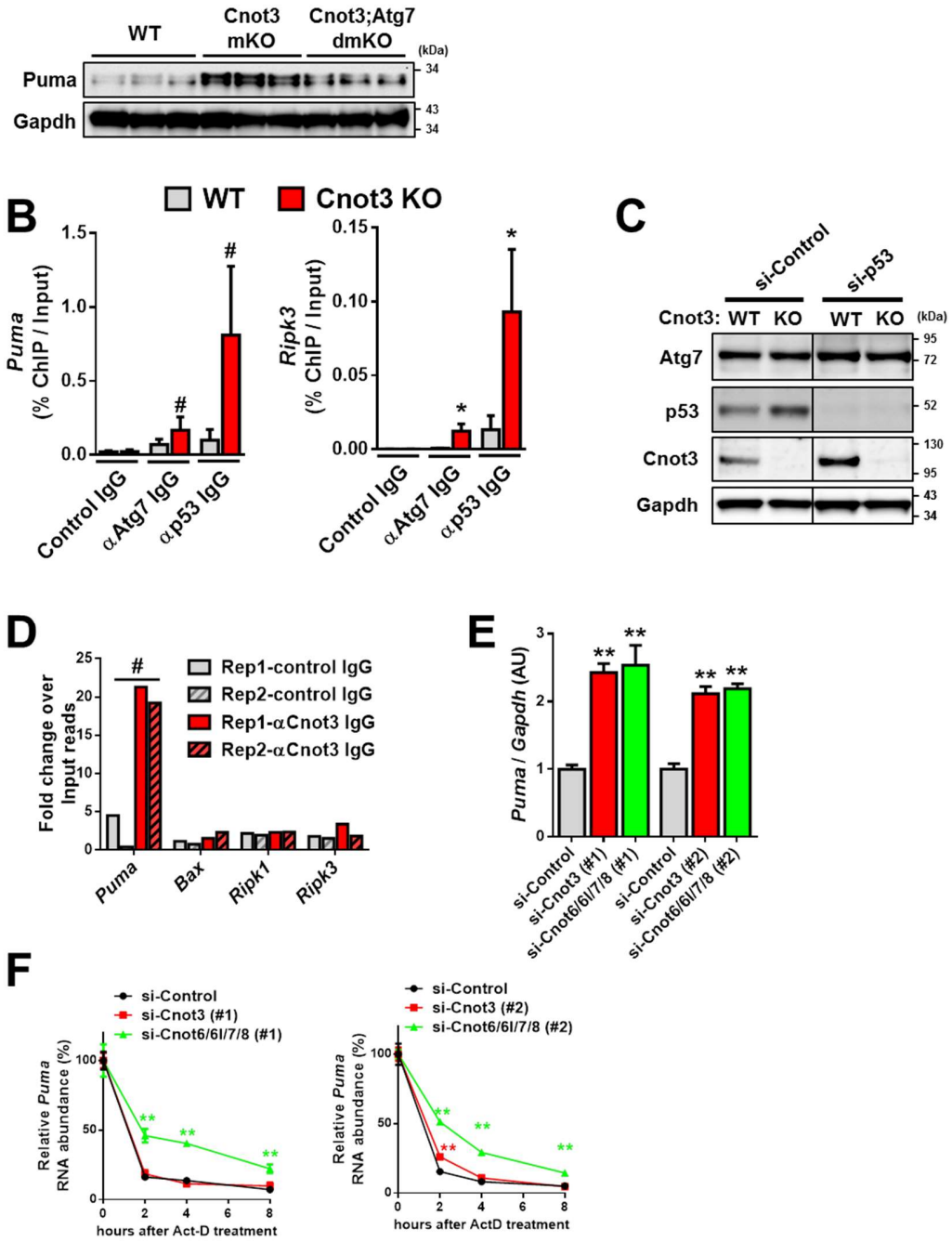

Fig. S11. Expression of cell death-associated genes in Cnot3 mKO mice.

A, Western Blot of Puma in the hearts of WT, Cnot3 mKO and Cnot3;Atg7 dmKO mice at 18 days old. Each lane represents an individual mouse. **B,** Chromatin immunoprecipitation (ChIP) using anti-Atg7 IgG, anti-p53 IgG or control IgG from Cnot3 KO MEF lysates. qPCR analysis of the gene locus close to the transcription starting site of *Puma* or *Ripk3* was performed. N=3 independent experiments. #P< 0.1,

*P < 0.05, one-tailed paired Student's *t*-test. **C**, Western blot for Atg7, p53 and Cnot3 in WT or Cnot3 KO MEFs transfected with si-p53. N=2 independent experiments. **D,** mRNAs in Cnot3 IgG (αCnot3) RIP or control IgG RIP, normalized to input, for two biological replicates (Rep1 and Rep2). #; *Puma* was selected as a gene enriched in Cnot3 RIP by R bioconductor package edgeR with the criteria of FDR < 0.05, cpm for mean Input > 0.1 and αCnot3 RIP/Input > $2^{0.5}$. **E,** qRT-PCR for *Puma* mRNA expression in cardiomyocytes transfected with siRNAs for control (N=6), Cnot3 (N=3) or combinations of Cnot6, Cnot6l, Cnot7 and Cnot8 siRNAs (N=3). N=2 independent experiments with two different siRNAs for Cnot3, Cnot6, Cnot6l, Cnot7 and Cnot8. **F,** mRNA stability of *Puma* mRNA in cardiomyocytes was analyzed after actinomycin D treatment. N=3 independent experiments with two different siRNAs for Cnot3, Cnot6, Cnot6l, Cnot7 and Cnot8. All values are means ± SEM. $^{\#}$P < 0.1, *P < 0.05, **P < 0.01, unpaired two-tailed Student's *t*-tests otherwise mentioned.

Table S1. Primer list

Analysis	Gene	5' primer	3' primer
qRT-PCR	*Ulk1*	5'-CGTCCTCCAAGACGCTGTAT-3'	5'-CCTGTTGCTTTCCTCCAAAG-3'
	Pik3c3	5'-AGAGCGTCCACGCACTGT-3'	5'-TCCCCTTTCATTTTCTCCAGT-3'
	Becn1	5'-ACCAGCTGGACACTCTCAGCTCAA-3'	5'-GCAGCTGCTCACTGTCATCCTC-3'
	Atg5	5'-TTGACGTTGGTAACTGACAAAGT-3'	5'-TGTGATGTTCCAAGGAAGAGC-3'
	Atg7	5'-GCTGCTGAGATCTGGGACAT-3'	5'-GAGATGTGGAGATCAGGACCAG-3'
	Atg12	5'-TGAATCAGTCCTTTGCCCCT-3'	5'-CATGCCTGGGATTTGCAGT-3'
	Map1lc 3b	5'-GTGGAAGATGTCCGGCTCAT-3'	5'-TGGTCAGGCACCAGGAACTT-3'
	Sqstm1	5'-GCTGCCCTATACCCACATCT-3'	5'-CGCCTTCATCCGAGAAAC-3'
	Trp53	5'-GGACCATCCTGGCTGTAGGTAG-3'	5'-CGAGGCTGATATCCGACTGTGA-3'
	Cnot1	5'-CAGAACCTGGCTGTCCACCTAGC-3'	5'-TGCCTCAGTGTTCGCCTCA-3'
	Cnot3	5'-TATGAAGAGAGTGCGTCTGTAGGGCAGGG-3'	5'-TCTTCAAACTGCTCCACCCCTTCGG-3'
	Cnot6	5'-CACATTGGGCAGAGCTTGAAATAA-3'	5'-GATGCAAAGCTGTCAAGTGAGTGAG-3'
	Cnot6l	5'-ACGGGTGTTGCCTTATGAACTTG-3'	5'-AAGTTCAGTAGCTTTCGGGTTCCA-3'
	Cnot7	5'-TTTGGGCTTGTAACCTGGATGAA-3'	5'-GTCTTGCAACAACGCCTGGA-3'
	Cnot8	5'-CCCGTCCATTTACGATGTGAAATAC-3'	5'-ACTTGGCATCGTCAATACTGTCCTC-3'
	Gapdh	5'-CTGCACCACCAACTGCTTAG-3'	5'-GTCTTCTGGGTGGCAGTGAT-3'
	18S	5'-AAACGGCTACCACATCCAAG-3'	5'-CCTCCAATGGATCCTCGTTA-3'
	Tbp	5'-GCTCTGGAATTGTACCGCAG-3'	5'-GGATTGTTCTTCACTCTTGGCTC-3'
ChIP	*Puma*	5'-AGCACCCCGATTCCCGAAGCTGCTT-3'	5'-TGTAAACAAACCCGCCAGACCGCTG-3'
	Ripk3	5'-CACCACATGCATGGTCATGCACA-3'	5'-ACAGACCAGGTTGACTCAAACTCAC-3'
Poly(A) length assay	*Ulk1*	5'-TCTTCCTTAGTCACCCTATGACCTCC-3'	5'-GAAACACAAAAGGGGGAGACTCAC-3'
	Pik3c3	5'-CTGCTGTGTACTAAAGACATCAAAG	5'-TCAGAGGGTAAAATGCTTTACTGT

		-3'	TTC-3'
	Becn1	5'-TAGCAAAGAACCCTGCCATAG-3'	5'-CACGTCGCACACAGTATCA-3'
	Atg5	5'-GGCTCCTGGATTATGTCATTGTTG-3'	5'-GCATACTCAGATGGGTTGACATTC-3'
	Atg7	5'-AACAAACTAGTGGCTATTAATGCGG-3'	5'-TAAAGACCATCATTACGCTGTGC-3'
	Atg12	5'-AGGTCATGCAGGGAATAGTCACAG-3'	5'-CTGGTAAAAATGTTTCAAATTCAAGTTTAT-3'
	Map1lc 3b	5'-ATGGACTGAAGCCAGCATAG-3'	5'-CAGGTTCGTTGTGCCTTTATTAG-3'
	Sqstm1	5'-CCTGACAACCCGTGTTTCCTTTAT-3'	5'-CAGGTTACTTACAAACCAAGTCAGAGG-3'
	Gapdh	5'-CTCCCACTCTTCCACCTTCGA-3'	5'-CTAGGCCCCTCCTGTTATTATGG-3'

Table S2. siRNA list

siRNA	siRNA target sequence
si-Cnot3 (#1)	5'-GAAGGAGATTAAGAAGCTA-3'
si-Cnot3 (#2)	5'-CTAAGACCATCACAGATGA-3'
si-Cnot6 (#1)	5'-GGCTAATGCTCATATGCAT-3'
si-Cnot6 (#2)	5'-CTATGATGTTCCTCTCAGA-3'
si-Cnot6l (#1)	5'-CCAATAAACTCAGAAGTTT-3'
si-Cnot6l (#2)	5'-GTGTTACAATGTGTTATGT-3'
si-Cnot7 (#1)	5'-GTTATGACTTTGGCTATTT-3'
si-Cnot7 (#2)	5'-GGTTATGACTTTGGCTATT-3'
si-Cnot8 (#1)	5'-CCATAGATCTGCTTGCAAA-3'
si-Cnot8 (#2)	5'-GCAATGTTGATCTTCTTAA-3'
si-Atg7	5'-CTGTGAACTTCTCTGACGT-3'
si-p53	5'-CCACTACAAGTACATGTGT-3'